



HAL
open science

Flux estimation, temporal trends and source determination of trace metal contamination in a major tributary of the Seine estuary, France

Thomas Gardes, Maxime Debret, Yoann Copard, Alexandra Coynel, Julien Deloffre, Matthieu Fournier, Sidonie Révillon, Jean Nizou, Anne-Lise Develle, Pierre Sabatier, et al.

► To cite this version:

Thomas Gardes, Maxime Debret, Yoann Copard, Alexandra Coynel, Julien Deloffre, et al.. Flux estimation, temporal trends and source determination of trace metal contamination in a major tributary of the Seine estuary, France. *Science of the Total Environment*, 2020, 724, pp.138249. <10.1016/j.scitotenv.2020.138249>. <hal-02556187>

HAL Id: hal-02556187

<https://normandie-univ.hal.science/hal-02556187v1>

Submitted on 20 May 2022

HAL is a multi-disciplinary open access archive for the deposit and dissemination of scientific research documents, whether they are published or not. The documents may come from teaching and research institutions in France or abroad, or from public or private research centers.

L'archive ouverte pluridisciplinaire HAL, est destinée au dépôt et à la diffusion de documents scientifiques de niveau recherche, publiés ou non, émanant des établissements d'enseignement et de recherche français ou étrangers, des laboratoires publics ou privés.



Distributed under a Creative Commons CC BY-NC 4.0 - Attribution - Non-commercial use - International License

1 Flux estimation, temporal trends and source determination of 2 trace metal contamination in a major tributary of the Seine 3 estuary, France

4
5 Thomas Gardes^{1,2,*}, Maxime Debret¹, Yoann Copard¹, Alexandra Coynel³, Julien Deloffre¹,
6 Matthieu Fournier¹, Sidonie Revillon⁴, Jean Nizou⁴, Anne-Lise Develle⁵, Pierre Sabatier⁵,
7 Stéphane Marcotte⁶, Edouard Patault¹, Quentin Faivre⁷, Florence Portet-Koltalo²

8
9 ¹Normandie Univ, Rouen, UNIROUEN, UNICAEN, CNRS, M2C, 76000 Rouen, France.

10 ²Normandie Univ, Rouen, UMR CNRS 6014 COBRA, 55 Rue Saint Germain, 27000 Evreux, France.

11 ³Université de Bordeaux, UMR EPOC CNRS 5085, 33615 Pessac, France.

12 ⁴IFREMER, IUEM Place N. Copernic, F-29280 Brest, France.

13 ⁵Université Grenoble Alpes, Université Savoie Mont Blanc, CNRS, EDYTEM, 73000 Chambéry, France.

14 ⁶Normandie Univ, Rouen, INSA de Rouen, UMR CNRS 6014 COBRA, Avenue de l'Université, 76801 Saint-
15 Etienne-du-Rouvray Cedex, France.

16 ⁷Université de Tours, EA 6293 GÉHCO, Parc de Grandmont, 37200 Tours, France.

17 *Corresponding author: thomas.gardes1@univ-rouen.fr

19 1. Introduction

20
21 Trace metal and metalloid elements (TMM) are naturally present in rivers as a result of
22 mechanical erosion processes or chemical alteration of uncontaminated rocks and soils. They
23 also originate from multiple sources related to anthropogenic activities resulting in the
24 contamination of rivers to varying degrees of severity (Salomons and Forstner, 1984).
25 Anthropogenic impacts are sometimes very old and may date back to the Roman era (Elbaz-

26 Poulichet et al., 2011), the Bronze Age (Elbaz-Poulichet et al., 2020), or even prehistory
27 (Chiaradia et al., 2003). However, many studies agree that the impacts from the last 150
28 years, since the industrial revolution of western countries, have been much more significant
29 (Foster and Charlesworth, 1996). Releases of TMM can be in dissolved and/or particulate
30 form. Particulate discharges may be transported to the lower reaches of a watershed
31 depending on hydraulic conditions, leading to the storage of these particles in accumulation
32 areas within rivers, such as reservoirs behind dams, floodplains or ponds (Foster and
33 Charlesworth, 1996). Using stored sediments, the reconstruction of temporal trends of metal
34 contamination within a watershed is possible when the latter are undisturbed. Stored
35 sediments with high accumulation rates (e.g., $\geq 1 \text{ cm y}^{-1}$) are only slightly affected by the early
36 diagenesis process (Callender, 2000), thus these sediments can be used to trace temporal
37 trends of metal contamination. This has been done for several large French rivers (e.g.,
38 Garonne River: Grousset et al., 1999; Audry et al., 2004; Seine River: Le Cloarec et al., 2011;
39 Ayrault et al., 2012; Loire River: Grosbois et al., 2012; Dhivert et al., 2016).

40 The Eure River in Normandie, is a major tributary of the Seine estuary and is part of the
41 Seine River watershed. This watershed is known for a history of significant metal
42 contamination within its fluvial (Le Cloarec et al., 2011) and estuarine parts (Chiffolleau et al.,
43 2012; Vrel, 2012).

44 The objective of this study is to assess and characterise the anthropogenic impacts within the
45 Eure River watershed over the last 80 years. The quantification of current inputs from the
46 Eure watershed into the Seine estuary was determined through TMM concentrations on
47 suspended particulate matter (SPM), to enable determination of particulate metal flux. The
48 reconstruction of TMM temporal trends was undertaken using sediment cores collected in the
49 lower reaches of the watershed. The determination of natural values of TMM within the
50 watershed allowed the assessment of current and past anthropogenic impacts. The magnitude

51 of the impact could also be traced over time based on the estimation of past theoretical flux.
52 The sources of the recorded contamination were determined by reconstructing the industrial
53 history of the watershed and using Pb isotope ratios.

54

55 **2. Material and Methods**

56

57 2.1. Characteristics of the Eure watershed

58

59 The Eure River is a tributary of the Seine estuary, regulated upstream by the Poses Dam
60 (Figure 1A). The Eure River watershed (6,017 km²) is the fourth largest tributary of the Seine
61 River watershed in terms of surface area. It falls behind the Yonne, Marne and Oise
62 watersheds but is the first contributing watershed in the estuarine section (i.e., the last 150 km
63 before the mouth to the Channel). It is based on a chalk formation of the Upper Cretaceous,
64 covered by Tertiary sandy-clay deposits and more recent deposits dating back to the
65 Quaternary period (Quesnel, 1997; Laignel et al., 1998). The Eure River waters are
66 characterised by a conductivity of $568 \pm 52 \mu\text{S cm}^{-1}$, a pH equal to 8.1 ± 0.2 and a mean
67 temperature of $13 \pm 5 \text{ }^\circ\text{C}$ on the period from 1971 to 2019 (www.naiades.eaufrance.fr).
68 Moreover, the Eure River has a mean annual flow (Q_{mean}) of $22.13 \pm 6.69 \text{ m}^3 \text{ s}^{-1}$ based on the
69 period from 1971 to 2019 (www.hydro.eaufrance.fr). It is the fifth largest tributary of the
70 Seine watershed in terms of flow and its two major tributaries are the Avre and Iton rivers
71 (Figure 1B).

72

73 2.2. Field Sampling Methods

74

75 2.2.1. *Description of core sites and sampling methodology*

76

77 Les Damps Pond is upstream of the Eure River spillway (Figure 1C). The pond, with an
78 average depth of 50 cm and spanning an area less than 1 ha, continually accumulates SPM
79 from the Eure watershed (Figure 1D). As the site is 2 km upstream of a spillway (vertical
80 height: ~3 m), the tides have no noticeable effect, even in the case of a high tidal coefficient.

81 The Martot Pond, spanning an area of ~7 ha, is located in the lower reaches of the study
82 area (Figure 1C). Unlike Les Damps Pond, this pond is affected by the Seine estuary during
83 tidal flows through the Eure River outlet. However, the impact of the tide is limited and
84 temporally variable, as its flow persists for about 3 h and does not occur every day. In
85 addition, the Martot Dam, located 200 m downstream of the Martot Pond, prevented tidal
86 flows for tidal coefficients lower than 70, until its removal in October 2017 (Figure 1E). Thus,
87 to ensure Martot Pond was not impacted by the Seine River, results from this site were
88 compared with those from Les Damps Pond. The Martot Dam also regulated the water level
89 in the river, and the river was continuously connected to the Martot Pond, even during periods
90 of low flow.

91 The La Forge Pond, located upstream of the Eure watershed, is crossed by the Avre River and
92 is less than 10 km downstream of the headwaters of the Avre River (Figure 1F). This pond
93 was constructed in anticipation of iron and steel activities during the seventeenth century. It is
94 at the outlet of a watershed spanning less than 14 km² where the geology is similar to that of
95 the entire watershed, i.e., an Upper Cretaceous formation composed of flint clay (Turonian)
96 and sand (Cenomanian) outcropping near the river.

97 Sediment cores were extracted using a UWITEC® gravity corer and PVC tubes with a
98 diameter of 90 mm (e.g., Sabatier et al., 2014). The water-sediment interface was preserved
99 during coring. Coring was carried out in the following dates and locations:

100 - January 2015 (DAM15-02 core) and January 2017 (DAM17-02 core) for Les Damps Pond;

101 - January 2015 (MAR15-01 core) and February 2016 (MAR16-02 core) for Martot Pond; and
102 - June 2017 (FOR17-02 core) for La Forge Pond.

103 The characteristics of sediment cores are listed in Table 1.

104

105 2.2.2. *Measurement of flow and turbidity*

106 Streamflow of the Eure River (Q_{water} ; $\text{m}^3 \text{s}^{-1}$) was directly measured using an Argonaut-
107 SL3000 current meter (Side-Looking Doppler Current Meters; SonTeck®) installed on the
108 left bank of the Eure River at the Les Damps site. Measurements were taken at 15 min
109 intervals from 27 January 2017 to 22 May 2018 (Figure 1D).

110 Turbidity (NTU) was measured using a SAMBAT multi-parameter probe (with self-cleaning
111 sensors; NKE Instrumentation®) installed in the channel 90 cm below the surface at the Les
112 Damps site. Measurements were taken at 15 min intervals during the same period as that of
113 streamflow (Figure 1D).

114

115 2.2.3. *SPM sampling*

116 SPM were collected using an home-made time-integrated mass-flux sampler (TIMS), the
117 design of which was based on Phillips et al. (2000) and Russell et al. (2000) (Figure S1 in
118 supplementary materials). The central tube (1 m long, diameter of 10 cm) and the two outer
119 inlet and outlet pieces are made of PVC. The pipe has a diameter of 4 mm, allowing water to
120 enter and exit, is made of nylon. The assembly of the parts and waterproofing of the central
121 tube was undertaken using O-rings without glue. The TIMS were installed on a raft in the
122 channel 90 cm below the surface at the Les Damps site, at the same depth as the turbidity
123 sensor (Figure 1D). All TIMS changeover dates are shown in italics in Figure 2A.

124

125 2.3. Analytical Methods and data processing

126

127 *2.3.1. Grain size analysis*

128 Grain size distribution can influence the behaviour of chemical substances. Short-lived
129 radionuclides (^{210}Pb , ^{137}Cs , and ^{241}Am) are preferentially adsorbed to fine particles (He and
130 Walling, 1996) as metallic and metalloid elements (Salomons and Forstner, 1984; Horowitz
131 and Elrick, 1987; Brüggemann, 1995). Thus, grain size distribution can have a considerable
132 impact on chronology and TMM concentrations in sediment cores (He and Walling, 1996).

133 The grain size distribution of sediment cores was measured by laser diffraction (LS 13320
134 Particle Size Analyser Beckman Coulter™) across a range 0.04–2000 μm . Measurements
135 occurred every cm by integrating 1 cm on the DAM15-02 and MAR15-01 cores.

136

137 *2.3.2. Total organic carbon analysis*

138 Total organic carbon (TOC) and the extent of organic matter (OM) degradation can
139 influence TMM concentrations as some TMM have a strong affinity to TOC (Tseng et al.,
140 2001; Audry et al., 2006; Masson et al., 2011; Petit et al., 2013; Coynel et al., 2016). As such,
141 TOC contents are needed to determine whether variations in TMM in the sediment cores are
142 related to anthropogenic activities.

143 Sediment Cores were analysed using Rock-Eval 6 (RE6) pyrolysis at the ISTO laboratory,
144 University of Orléans (“Turbo” model RE6 pyrolyzer, Vinci Technologies), as per the method
145 described in Copard et al. (2006). TOC and the OM quality were measured on the DAM17-02
146 and MAR15-01 cores at intervals of 2 and 1 cm, respectively.

147

148 *2.3.3. XRF core scanning (XRF-CS)*

149 X-Ray fluorescence spectrometry (XRF) was used to semi-quantitatively determine the major
150 and trace element variations of sediment deposits (Richter et al., 2006). The XRF core

151 scanning data can be used to describe particulate TMM contamination in sediment cores
152 (Lepland et al., 2010; Hennekam et al., 2019; Elbaz-Poulichet et al., 2020). The data
153 presented were normalized by Ti to remove possible variations due to detrital inputs (Duan et
154 al., 2014; Bábek et al., 2015). Ti was considered a better “normalizing element” than Al,
155 which is used in coagulation/flocculation processes in wastewater treatment plants.

156 The relative contents of TMM were measured using an Avaatech XRF core scanner
157 (EDYTEM, University of Savoie Mont Blanc). Measurements were taken every 5 mm for the
158 MAR15-01 and DAM17-02 cores and every 2 mm for the MAR16-02 core.

159

160 *2.3.4. Particulate trace metal and metalloid analysis*

161 Microwave-assisted sediment digestion for particulate TMM analyses (for As, Cd, Cu, Cr,
162 Ni, Mn, Pb, Zn), was performed on samples collected from the MAR16-02 and DAM17-02
163 cores. This consisted of 0.5 g of dry, powdered and homogenised sediment with aqua regia
164 (HNO₃: 3 mL TraceMetal™ Grade; HCl: 9 mL TraceMetal™ Grade, Fisher Scientific®).
165 Following pseudo-total mineralization (residual fractions containing silica particles being
166 only partially digested), solutions were diluted in 100 mL Milli-Q® water. Particulate TMM
167 concentrations were measured using inductively coupled plasma-atomic emission
168 spectroscopy (ICP-AES, iCAP 6000 Series, Thermo Fischer®) with external calibration. The
169 accuracy and precision of measurements were verified with a certified reference material
170 (Trace Element on Fresh Water Sediment CNS301-04-050, Sigma Aldrich) and results
171 showed recoveries of $\geq 88\%$ with a precision of $\sim 3.1\%$.

172 Total digestions, including residual fractions, were performed on selected samples, collected
173 at different depths for the DAM17-02 core, corresponding to the highest and lowest levels
174 determined by ICP-AES. They were also conducted on sediment collected at the bottom of the
175 FOR17-02 core. Representative samples consisting of 30 mg of dry, powdered and

176 homogenized sediment, were digested in closed polypropylene (PP) reactors (DigiTUBEs®,
177 SCP SCIENCE) in a heating block (2 h at 115 °C) with 1.5 ml HCl (12 M Suprapur®,
178 Merck), 0.75 ml HNO₃ (14 M Suprapur®, Merck) and 2.5 ml HF (22 M Suprapur®, Merck),
179 as described in previous studies (e.g., Coynel et al., 2016). Particulate TMM concentrations
180 were measured by inductively coupled plasma-mass spectroscopy (ICP-MS, X7 Series 2,
181 THERMO) with external calibration under standard conditions. The accuracy and precision of
182 measurements were verified with certified reference materials (NCS DC 2702, CRM 8704,
183 BCR 667) and results showed recoveries of $\geq 93\%$ with a precision of $\leq 4\%$ (relatively
184 standard deviation; RSD). The concentrations (for Cr, Ni, Cu, Zn, As, Cd, and Pb) determined
185 by ICP-MS (total concentrations) were always consistent with those determined by ICP-AES
186 (pseudo-total concentrations) being 1.1 to 1.5 times higher than the latter.

187 Sediment samples from MAR15-01 (n=6) were analysed for Pb radiogenic isotopes.
188 Reagents used for digestion and chemical procedures were prepared from sub-boiled distilled
189 concentrated hydrochloric and nitric acids using a Cleanacids® device (Analab, France)
190 except HClO₄ (Suprapur®, Merck) Approximately 100 mg of sample was weighed and
191 dissolved in savillex® Teflon beakers in a mixture of HF (24 M, Cleanacids®, Analab),
192 HNO₃ (14 M, Cleanacids®, Analab), and HClO₄ (12 M, Suprapur®, Merck) for four days at
193 160 °C on a hot plate. After evaporation to dryness, samples were dissolved in aqua regia and
194 heated for 24 h at 130 °C. Pb fractions were chemically separated following conventional
195 column chemistry procedures described in Gale (1996). Pb isotopic compositions analyses
196 was conducted at the Pôle de Spectrométrie Océan (PSO) in Brest, France using a multi-
197 collector ICP-MS (MC-ICPMS, Neptune, Thermo Scientific). Pb isotope ratios were
198 corrected for instrumental mass fractionation and machine bias using the Tl doping method of
199 White et al. (2000) and SRM981 Pb standard bracketing for every three samples. Pb isotope
200 reproducibility, based on 21 replicate analyses of NIST (National Institute of Standards and

201 Technology) SRM981 was 0.0018 (2σ) for $^{206}\text{Pb}/^{204}\text{Pb}$ and $^{207}\text{Pb}/^{204}\text{Pb}$ and 0.0045 (2σ) for
202 $^{208}\text{Pb}/^{204}\text{Pb}$.

203

204 2.3.5. *Suspended particulate matter and particulate TMM flux determination*

205 To convert turbidity measurements into SPM concentrations (C_{MES} ; mg L^{-1}), an NTU-SPM
206 calibration line was established from SPM samples collected monthly at the Les Damps site
207 (Figure S2). Equation (1) of this calibration line ($R^2 = 0.85$) is:

$$208 \quad C_{MES} = 1.155 \times \text{Turbidity} \quad \text{Equation (1)}$$

209 The monthly SPM flux (F_{SPM} ; t month^{-1}) was then determined according to Equation (2):

$$210 \quad F_{SPM} = \sum Q_{water} \times C_{MES} \quad \text{Equation (2)}$$

211 Particulate TMM flux was estimated monthly over the sampling period based on the SPM
212 flux and TMM concentrations determined from the collected SPM.

213

214 2.3.6. *Enrichment factors calculation*

215 To assess the impact of anthropogenic activities based on concentrations in environmental
216 samples, these concentrations need to be standardised to reduce the influence of the
217 sedimentary matrix (Ackermann, 1980; Daskalakis and O'Connor, 1995). Normalisation is
218 based on a conservative trace element (i.e., not influenced by oxidation-reduction or
219 diagenesis processes in sediments). Variations are characterised in the fine fraction varying
220 proportionally with background concentrations, where most TMM are preferentially enriched.
221 This normalising element should not have anthropogenic inputs that alter its distribution. The
222 element Th is highly insoluble (Van Calsteren and Thomas, 2006), and is known to have a
223 strong negative correlation with particle size, which allows its effects to be corrected (e.g.,
224 Coynel et al., 2007; Larrose et al., 2010; Lanceleur et al., 2011a, 2011b; Le Cloarec et al.,
225 2011). In the literature, enrichment factors (EFs) are commonly used to estimate the impact

226 of anthropogenic activities on the natural cycle of trace elements. EFs were determined
227 according to Equation (3):

$$228 \quad EF = \frac{TE / RE}{TE_{ref. background} / Th_{ref. background}} \quad \text{Equation (3)}$$

229 TE and RE represent the concentration of TMM studied and the reference element (Th)
230 chosen for a given sample. $TE_{ref. background}$ and $RE_{ref. background}$ represent the natural content of
231 the studied element and the natural content of Th, respectively.

232

233 2.4. Core dating

234

235 2.4.1. Short-lived radionuclides

236 The dating of recent deposits within sediment cores and the estimation of sedimentation
237 rates was carried out using radioelements with short periods. The sedimentation rate was
238 determined from the activity of ^{210}Pb in excess ($^{210}\text{Pb}_{\text{ex}}$), by subtracting ^{226}Ra from the
239 $^{210}\text{Pb}_{\text{total}}$ (Goldberg, 1963). Artificial radioelements ^{137}Cs and ^{241}Am were used to identify
240 nuclear weapons tests to confirm the age model established from the $^{210}\text{Pb}_{\text{ex}}$ results. A peak
241 was observed in 1963 AD and in 1986 AD when the Chernobyl nuclear power plant accident
242 occurred (Appleby et al., 1991).

243 The activities of $^{210}\text{Pb}_{\text{ex}}$, ^{137}Cs and ^{241}Am were determined using gamma spectrometry with a
244 germanium spectrometer in ultra-low background noise settings at the Laboratoire Souterrain
245 de Modane (LSM). The age model was computed with *serac* R package
246 (<https://github.com/rosalieb/serac>, (Bruel and Sabatier, 2020)). The MAR15-01 core was
247 sampled from 0 to 80 cm at intervals of 2, 4, and 6 cm.

248

249 2.4.2. ^{14}C dating

250 ¹⁴C dating was conducted at the Poznań Radiocarbon Laboratory from organic macro
251 remains collected at the bottom (i.e., 68–69.5 cm interval) of the FOR17-02 core. The
252 IntCal13 calibration curve (Reimer et al., 2013) was used for ¹⁴C age calibration, and the
253 sample was determined to be from the period between 1646 and 1669 cal AD (Figure S3).

254

255 **3. Results and interpretation**

256

257 3.1. Determination of local geochemical background

258

259 The beginning of the FOR17-02 core (68–69.5 cm) was radiocarbon dated between 1646
260 and 1949 (1 sigma) with a maximum probability that it is between 1646–1669 (56%) and
261 1781–1798 (39%) (Figure S3). The 68–69.5 cm fraction was characterised by a median grain
262 (D_{50}) of 20.9 μm and a TOC content of 2.77% (dry weight; dw) (additional description of the
263 FOR17-02 core is provided in Figure S4).

264 The TMM concentrations of this sample are summarized in Table 2. In light of the small
265 geological variations within the Eure watershed and the sample being dated back to the pre-
266 industrial revolution period, the TMM concentrations are indicative of the geochemical
267 background (GB) of the Eure watershed. The choice of the GB in this study, differs from
268 some studies that have used levels measured at the bottom of sediment cores, considered
269 representative of the GB (e.g., Gascón Díez et al., 2017), or used a regional geochemical
270 baseline, representing levels measured prior to significant additional anthropogenic inputs, but
271 not corresponding with a regional GB (Larrose et al., 2010). In other cases, for example for
272 the Seine watershed (67,500 km²; Le Cloarec et al., 2011), the GB was the combination of
273 several average levels of TMM in fine sediments collected in forest streams draining a single
274 rock type (Horowitz et al., 1999; Thévenot et al., 2007).

275

276 3.2. Current behaviour of the Eure River

277

278 3.2.1. *Hydro-sedimentary behaviour*

279 The average flow in the Eure River was $22.0 \text{ m}^3 \text{ s}^{-1}$ at the Les Damps site in 2017. There
280 were no major flood events during this year, with the exception of the month of March when
281 streamflow reached $86.7 \text{ m}^3 \text{ s}^{-1}$, the highest in 2017. The beginning of 2018 was marked by a
282 50-year flood during which five flood peaks were recorded. Maximum flow values occurred
283 between late January and early February 2018, with streamflows close to $180 \text{ m}^3 \text{ s}^{-1}$ (Figure
284 2A).

285 The monthly SPM flux also followed the same trend as streamflow. The maximum monthly
286 flux in 2017 was $4.27 \times 10^4 \text{ t}$ in March 2017, while the minimum flux was 812 t in July 2017.
287 The total flux for 2017 was $10.8 \times 10^4 \text{ t}$, with a specific sediment yield (SSY) of about 18 t
288 $\text{km}^{-2} \text{ y}^{-1}$. The 2018 flood (January–March) transported $36.0 \times 10^4 \text{ t}$ of SPM, of which more
289 than half ($20.4 \times 10^4 \text{ t}$) passed through in January (Figure 2A).

290

291 3.2.2. *Evolution of TMM concentrations*

292 Figure 2B presents the changes in TMM and Mn concentrations over the entire sampling
293 period at the Les Damps site. According to the correlation matrix, most of the TMM and Mn
294 did not show any correlation with Q_{mean} , SPM_{mean} and dw (for SPM collected by TIMS),
295 indicating that their concentration variations are not directly related to the hydro-sedimentary
296 behaviour of the Eure River, nor to the mass of SPM collected (Figure S5). Only As showed
297 positive but low correlations ($0.36 < R < 0.56$) with these three parameters. Overall, TMM
298 and Mn were positively correlated with each other ($0.42 < R < 0.99$), but some elements such
299 as V, As and Th showed particularly strong positive correlations ($0.90 < R < 0.99$) and

300 therefore co-variated during the sampling period. This was particularly the case during the 50-
301 year flood from 22 January to 19 February, 2018. During this time, only V, As and Th
302 reached maximum levels at 55.3, 8.45 and 6.44 mg kg⁻¹, respectively (Figure 2B). Chromium,
303 Co, Ni and Mn had strong correlations between them ($0.60 < R < 0.89$) and with Th or V for
304 Cr, Co and Ni ($0.73 < R < 0.88$). Lead was correlated with Ag ($R = 0.89$) and Sb ($R = 0.70$),
305 and like Ag, was negatively correlated with Q_{mean} , SPM_{mean} and dw . This resulted in low
306 levels of Pb and Ag during the flood with Ag having reached its lowest concentration of 0.75
307 mg kg⁻¹ (Figure 2B).

308 The average concentrations of V, As and Th based on the SPM were close to those of the
309 GB of the Eure watershed (Table 2). The other TMM had average concentrations higher than
310 those of the GB. Over the entire sampling period, Cu, Cd and Pb measured at levels 12, 18,
311 and 14 times higher than the GB, respectively.

312 For concentrations of TMM normalised by Th, the average ratios were found to be higher
313 than those calculated for the GB, with the exception of V, As and Th. This indicates that the
314 inputs of As within the watershed were not of anthropogenic origin. For the other TMM, it is
315 likely that one or more additional anthropogenic sources releasing TMM into the river or that
316 old contaminated and stored/trapped sediments/soils have been remobilised. This may be
317 likely to occur during flood or work periods, and transit through the Eure River.

318

319 3.2.3. *Particulate TMM flux*

320 The total monthly flux of particulate TMM are listed in Table 3. In 2017, 50% of TMM flux
321 was transported between January and May as per the water flux. It may also have been
322 transported between January and April for V, As, Ag, Cd, Sb and Th as per the SPM flux.
323 Maximum flux occurred in March during the episodic flood. The flood in 2018 had a major
324 impact on the transport of TMM within the watershed. Indeed, between January and March,

325 the TMM flux was 3.3 times greater on average compared to the whole of 2017. Note that this
326 average ratio was 1.9 times if only the month of January is considered. Specifically, this
327 behaviour was more pronounced for V, Co, Ni, Cu, As, Th (ratio of 3.5–4.0) and less
328 pronounced for Ag (ratio of 2.0) and Pb (ratio of 2.8). During the flood event, more than half
329 ($57 \pm 1\%$) of the flux occurred in January, including the particulate flux for all the TMM. The
330 TMM with the highest flux was Zn and Pb, followed by Cr and Cu (Table 3).

331 While variations in TMM contents are independent of the hydro-sedimentary behaviour of
332 the Eure River, variations in TMM flux, such as increases during flood periods, are due to the
333 increase in hydro-sedimentary inputs. These streamflow increases are thus indicative of the
334 increased erosion of soils or sediments stored in the river.

335

336 3.3. Past contamination in the Eure River watershed

337

338 3.3.1. *Sedimentary characteristics*

339 The sediment deposits of the DAM15-02 core (Les Damps Pond) had a grain size
340 distribution mainly centred around D_{50} , equal to $29.5 \pm 6.7 \mu\text{m}$, with a constant TOC content
341 of $5.36 \pm 0.47\%$ (Figure 3A). The sediment deposits of the MAR15-01 core (Martot Pond),
342 were characterised by two sedimentary facies called U2 (77–138 cm) and U1 (0–77 cm)
343 (Figure 3B). Along U2, the grain size distribution was centred around a low D_{50} equal to 13.8
344 $\pm 7.0 \mu\text{m}$, and there was a low and constant mean TOC content ($1.75 \pm 0.33\%$). Along U1, the
345 grain size distribution was also centred around a D_{50} of $33.9 \pm 7.8 \mu\text{m}$, and the mean TOC
346 content ($3.88 \pm 1.49\%$) appeared to increase slightly within U1 towards the interface. There
347 were particularly high values close to the interface (TOC = $8.26 \pm 0.19\%$ between 9 and 12
348 cm) (Figure 3B). The D_{50} and mean TOC content were higher in the Martot Pond for U1
349 compared to U2. However, the D_{50} of U1 in the Martot Pond and that of Les Damps Pond

350 were comparable, while the mean TOC content was higher in Les Damps Pond (Gardes et al.,
351 2020a).

352

353 3.3.2. Age model

354 The activity of $^{210}\text{Pb}_{\text{ex}}$ was measured up to 80 cm (U1 of MAR15-01 core) and was found to
355 decrease almost continuously with depth (Figure 4A). A sedimentation rate of $12.73 \pm 2.2 \text{ mm}$
356 y^{-1} ($R^2 = 0.60$) was estimated using the ‘constant flux, constant sedimentation rate’ (CFCS)
357 model (Krishnaswamy et al., 1971). The ^{137}Cs and ^{241}Am activities peaked at 60 and 58 cm,
358 respectively, corresponding to the maximum fallout from atmospheric nuclear weapon testing
359 in 1963 (Robbins and Edgington, 1975). There was also a peak in the ^{137}Cs activity at 40 cm,
360 potentially related to the Chernobyl accident in 1986 (Appleby et al., 1991) (Figure 4B). The
361 first identification of ^{137}Cs activity dated 1955 (Pennington et al., 1973) corresponded to a
362 depth of 71 cm. From the mean sedimentation rate obtained by the $^{210}\text{Pb}_{\text{ex}}$, an age model was
363 constructed that was consistent with the artificial radionuclide data (Figure 4C). The transition
364 between U1 and U2 was dated at $1954 \pm 10 \text{ y}$. However, the history of the study site suggests
365 that around 1939, the Martot Pond, then connected to the Seine River, was disconnected from
366 the Seine River and subsequently connected to the Eure River in the following years. Thus,
367 the U2 facies corresponds to sedimentary deposits from the Seine watershed while the U1
368 facies corresponds to contributions from the Eure watershed since the 1940s (Gardes et al.,
369 2020a).

370 As the MAR16-02 and DAM17-02 cores on which the TMM were measured (see Section
371 3.3.3) were not dated, an age model was defined using the MAR15-01 core. This was done by
372 linking the peaks of the Pb/Ti and Zn/Ti ratios together based on analogy, or using the U1/U2
373 transition level also visible along the MAR16-02 core (Figure S6). Among the several
374 parameters useful to correlate sediment cores, XRF data is interesting because of the

375 measurements resolution. In addition, Pb and Zn already showed distinct temporal trends in
376 the Martot and Les Damps Ponds, using XRF analysed. Indeed, high levels of Zn were
377 obtained in the 1950s-1960s whereas high levels of Pb were obtained in the 1990s,
378 corresponding to the “middle” of the sediment cores and approximatively to the top of the
379 sediment cores, respectively (Gardes et al., 2020a). The results indicated average
380 sedimentation rates of 11.3 mm y^{-1} for the MAR16-02 core and 12.2 mm y^{-1} for the DAM17-
381 02 core.

382

383 *3.3.3. Evolution of the TMM concentrations along sediment cores*

- 384 • MAR16-02 core

385 The TMM concentrations in the MAR16-02 core were measured for U1 (0–77 cm),
386 corresponding to inputs from the Eure River into the Martot Pond, and for the last length of
387 U2 (77–90 cm), corresponding to inputs from the Seine River. Chromium, Mn, Ni, Cu, Zn
388 and Cd concentrations increased from the transition U2/U1 (Seine Unit/Eure Unit) with a
389 peak in the late 1950s ($\text{Cr} = 211 \pm 1 \text{ mg kg}^{-1}$; $\text{Mn} = 2198 \pm 9 \text{ mg kg}^{-1}$; $\text{Ni} = 48.9 \pm 0.1 \text{ mg kg}^{-1}$;
390 $\text{Cu} = 399 \pm 4 \text{ mg kg}^{-1}$; $\text{Zn} = 905 \pm 1 \text{ mg kg}^{-1}$; $\text{Cd} = 42.3 \pm 0.1 \text{ mg kg}^{-1}$), and in the mid-1950s
391 for Mn. Levels of Cr, Mn, Ni, Zn, and Cd remained high until the early 1960s and then
392 declined, in stages, until the late 1980s. From the 1980s onwards, the contents of Cr, Mn, Ni,
393 Cu, Zn and Cd remained stable ($\text{Cr} = 56.9 \pm 0.3 \text{ mg kg}^{-1}$; $\text{Mn} = 234 \pm 1 \text{ mg kg}^{-1}$; $\text{Ni} = 22.6 \pm$
394 0.1 mg kg^{-1} ; $\text{Cu} = 94.2 \pm 0.5 \text{ mg kg}^{-1}$; $\text{Zn} = 311 \pm 1 \text{ mg kg}^{-1}$; $\text{Cd} = 3.78 \pm 0.03 \text{ mg kg}^{-1}$) (Figure
395 5A). Arsenic concentrations had a peak in the U2 facies and then decreased during the
396 transition from the Seine Unit to Eure Unit with a peak in the late 1950s of $12.2 \pm 0.2 \text{ mg kg}^{-1}$.
397 Concentrations of As then decreased until the end of the 1980s, stabilising around a mean
398 content of $4.12 \pm 0.23 \text{ mg kg}^{-1}$ up to the surface (Figure 5A). Pb concentrations increased
399 significantly from the late 1980s with a peak of $669 \pm 3 \text{ mg kg}^{-1}$ in the mid-2000s. During the

400 2010s the Pb concentrations declined rapidly but remained elevated and above levels
401 measured prior to the increase in the late 1980s (Figure 5A).

402

403 • DAM17-02 core

404 The evolution of TMM levels in the Les Damps Pond are similar to those obtained for the
405 Martot Pond, indicating a global signature of the watershed within these two ponds, not
406 impacted by local inputs (e.g., around the ponds). Indeed, the concentrations of Cr, Mn, Ni,
407 Cu, Zn, Cd were similar with the maxima during the 1960s and 1970s (Cr = 171 ± 1 mg kg⁻¹;
408 Mn = 1283 ± 2 mg kg⁻¹; Ni = 75.4 ± 0.2 mg kg⁻¹; Cu = 490 ± 1 mg kg⁻¹; Zn = 992 ± 3 mg kg⁻¹;
409 Cd = 54.6 ± 0.1 mg kg⁻¹). This was followed by a decrease until the 1990s before stabilising
410 within the most recent deposits (Cr = 39.0 ± 0.9 mg kg⁻¹; Mn = 140 ± 1 mg kg⁻¹; Ni = $17.0 \pm$
411 0.1 mg kg⁻¹; Cu = 67.2 ± 0.2 mg kg⁻¹; Zn = 279 ± 1 mg kg⁻¹; Cd = 3.34 ± 0.02 mg kg⁻¹)
412 (Figure 6). Chromium, Mn, Ni, Cu, Zn and Cd share similar trends suggesting a common
413 source for these TMM during the 1960s and 1970s. The maximum As concentration of $22.2 \pm$
414 0.2 mg kg⁻¹ was measured at the bottom of the DAM17-02 core around 1945. Levels then
415 gradually decreased and stabilised at 5.26 ± 0.14 mg kg⁻¹ from the 1990s (Figure 6). Pb
416 concentrations remained stable until the mid-1980s, then reached high concentrations during
417 the 1990s–2000 with peaks of 854 ± 8 mg kg⁻¹ in the early 1990s. Pb concentrations then
418 declined from the mid-2000s and reached concentrations close to those measured at the
419 beginning of the record. However, these were still higher than the lowest concentrations
420 obtained in the late 1960s (Figure 6).

421

422 3.4. Comparison between geochemical background values, past and current concentrations

423

424 The total TMM concentrations measured by ICP-MS for the DAM17-02 core are also listed
425 in Table 4. Vanadium and Th showed stable levels throughout the DAM17-02 core ($V = 45.4$
426 $\pm 5.4 \text{ mg kg}^{-1}$ and $\text{Th} = 5.18 \pm 0.62 \text{ mg kg}^{-1}$), these were close to the GB values of the Eure
427 River ($V = 43.2 \text{ mg kg}^{-1}$ and $\text{Th} = 3.96 \text{ mg kg}^{-1}$; Table 2) and also close to the estimated levels
428 for SPM (Figure 6). The temporal trends of V and Th confirm the absence of additional
429 anthropogenic inputs within the watershed. Arsenic is the only TMM for which the lowest
430 levels (corresponding to the most recent levels) were close to the GB value of 6.56 mg kg^{-1}
431 (Table 2) and the levels measured on the SPM (Figure 6). The temporal trends in As confirm
432 that there are no further anthropogenic additional inputs of As within the watershed. For the
433 other TMM, the overall estimated concentrations in the DAM17-02 core were always higher
434 than the GB values. Cobalt and Ag had similar trends to Cr, Mn, Ni, Cu, Zn or Cd and more
435 precisely to Cr and Zn with a peak concentration in the 1970s (Figure 6). The most recent and
436 oldest Cr, Co, Ni, Ag and Cd concentrations in the DAM17-02 core were close to those
437 measured on the SPM. In contrast, for Cu and Zn, only the most recent concentrations were
438 close to those measured on the SPM (Figure 6). Sb concentrations were similar to Pb with a
439 peak concentration in the early 1990s of 6.62 mg kg^{-1} . The Pb levels measured in the SPM
440 were slightly lower than those measured for the most recent deposits in the DAM17-02 core.

441 For all the TMM, the small differences in value between the estimated concentrations in
442 SPM and those measured in most recent sedimentary deposits show that sediment cores
443 collected were representative of SPM transfers in the Eure River.

444

445 3.5. Isotopic signature of Pb contamination

446

447 For the Seine Unit, where the Pb/Ti ratio was low (Figure S6), the values of the $^{206}\text{Pb}/^{207}\text{Pb}$,
448 $^{206}\text{Pb}/^{204}\text{Pb}$ and $^{208}\text{Pb}/^{204}\text{Pb}$ ratios were higher than those recorded in the Eure Unit and lower

449 for $^{208}\text{Pb}/^{206}\text{Pb}$. The 1990s constituted a period of high Pb concentrations, where the
450 $^{206}\text{Pb}/^{207}\text{Pb}$, $^{206}\text{Pb}/^{204}\text{Pb}$, $^{208}\text{Pb}/^{204}\text{Pb}$ ratios were low while the $^{208}\text{Pb}/^{206}\text{Pb}$ ratio was higher
451 than the 1960s. This decrease in the $^{206}\text{Pb}/^{207}\text{Pb}$, $^{206}\text{Pb}/^{204}\text{Pb}$, $^{208}\text{Pb}/^{204}\text{Pb}$ ratios and increase in
452 the $^{208}\text{Pb}/^{206}\text{Pb}$ ratio reflects a change in Pb source or inputs from a new source within the
453 sediment record, contributing to the increased Pb levels. From the 2000s onwards, the
454 $^{206}\text{Pb}/^{207}\text{Pb}$, $^{206}\text{Pb}/^{204}\text{Pb}$ and $^{208}\text{Pb}/^{204}\text{Pb}$ ratios increased slightly and $^{208}\text{Pb}/^{206}\text{Pb}$ remained
455 stable. This increase was confirmed for the ratios calculated in 2012 ± 0.5 y while the
456 $^{208}\text{Pb}/^{206}\text{Pb}$ started to decrease (Figure 5B). This increase and decrease for $^{208}\text{Pb}/^{206}\text{Pb}$,
457 corresponds to the decrease in Pb concentrations recorded in the Martot Pond (Figure 5A).
458 This reflects a reduction in the source contribution of Pb responsible for the elevated
459 concentrations and the strong modification of the isotope ratios during the 1990s and 2000s.
460 As such, there is a correlation between the temporal trend in Pb concentrations and that of Pb
461 isotopes, the latter reflecting a major source change for Pb in the sediment record.

462

463 **4. Discussion**

464

465 4.1. Evaluation of anthropogenic contribution

466

467 The use of EFs to assess the anthropogenic impact of contamination requires the selection of
468 a reference background. In some cases, the reference background used was a GB considered
469 representative of the whole watershed, as for example for the Seine watershed (Horowitz et
470 al., 1999; Thévenot et al., 2007; Le Cloarec et al., 2011), or the reference background was a
471 GB measured at the bottom of sediment cores (Section 3.1.). In other cases, to compensate for
472 the absence of a local GB, some studies have turned to the Upper Continental Crust (UCC)
473 values (Wedepohl, 1995). To assess anthropogenic impacts, EFs were calculated in our study

474 from the DAM17-02 core using two reference backgrounds, the local GB defined using the
475 FOR17-02 core and a reference level corresponding to the lowest concentration at the bottom
476 or top of the DAM17-02 core (Table 5). Although the variations in EFs were similar
477 regardless of the reference background, the lowest EFs were those calculated using the
478 reference level (with the exception of As). The strongest EFs were in the 1960–1970s for Cr,
479 Co, Ni, Cu, Zn, Ag, Cd.

480 For Cr, Cu, Zn and Cd, the maximum EFs calculated from the GB of the Eure watershed,
481 were higher than those for the Oise River, a tributary of the Seine River (Le Cloarec et al.,
482 2011) or the Lot River (with the exception of Zn), a tributary of the Garonne River, known for
483 its historical Cd contamination with industrial origin (Audry et al., 2004). These EFs were
484 still lower than those calculated for the lower reaches of the Seine River, with the exception of
485 Cu and Cd (Le Cloarec et al., 2011) but were higher or close to those obtained for other major
486 French rivers such as the Rhône (Ferrand et al., 2012) or Loire rivers (Grosbois et al., 2012;
487 Dhivert et al., 2016). This demonstrates that with regard to these TMMs, anthropogenic
488 pressures within the Eure watershed were higher than those recorded for Oise River, another
489 tributary of the Seine estuary and of the same register as those recorded within major French
490 river watersheds. Conversely, the EFs calculated for As from the reference level were higher
491 but of the same order of magnitude, than those calculated from the GB on the watershed
492 (Table 5). Sediments from the Eure River had a maximum EF at the beginning of the
493 sedimentary record (i.e., during the 1940s), which was lower than the maximum EF calculated
494 in the Oise River or the lower reaches of the Seine River (Le Cloarec et al., 2011). In terms of
495 Sb, the maximum EF (Table 5) was lower than those recorded in the Oise River or the lower
496 reaches of the Seine River (Le Cloarec et al., 2011) whereas for Pb, the maximum EF in the
497 Eure River was higher than most maximum EFs obtained for other watersheds including the
498 Oise (Le Cloarec et al., 2011), Lot (Audry et al., 2004), Rhône (Ferrand et al., 2012) and

499 Loire rivers (Grosbois et al., 2012). This highlights the high anthropogenic pressures on the
500 Eure watershed since the 1990s, compared to other French watersheds. Since the 1990s, all of
501 the TMM (except for Sb and Pb) were stable with relatively low concentrations (and EFs),
502 which may result from a significant reduction or a halt in additional discharges during the
503 1960–1970s period. This is assuming that a strong EF corresponds to strong anthropogenic
504 pressure. The lowest levels, considered the baseline within the sediment record, remain higher
505 compared to the GB of the watershed, with the exception of As. This suggests that
506 anthropogenic pressures within the watershed are now low but not null (Table 5). Due to the
507 multiple anthropogenic pressures that a watershed may experience, it can be assumed that soil
508 and sediments quality can only be degraded to pre-industrial revolution levels. As such, EF
509 from the bottom or top of sediment cores, which can be considered permanent anthropogenic
510 baseline, may seem more realistic for the evaluation of anthropogenic pressures in a
511 watershed. This makes it possible to distinguish between periods when anthropogenic
512 pressure is active via industrial, agricultural or even urban discharges, and periods when high
513 levels of TMM (in relation to GB) are solely due to the mechanical erosion of impacted soils
514 or re-suspension of contaminated sediments stored in the river. The remobilisation of
515 contaminated soils has already been observed in small wine-growing watersheds (Sabatier et
516 al., 2014) or those dominated by pastoralism (Bajard et al., 2018).

517

518 4.2. Current and theoretical past contributions

519

520 Over the period 1994–2003, Thévenot et al. (2007) estimated mean annual flux from the
521 Seine watershed to the Seine estuary for Cr, Cu, Zn, Cd and Pb. Assuming that TMM flux out
522 of the Seine watershed has not changed since this period, this flux out of the Eure watershed
523 for 2017 (Table 3) would be representative of 7, 8, 9, 10, and 16% of the total inputs (Seine

524 River + Eure River) of Cr, Cu, Zn, Cd and Pb into the Seine estuary, respectively (Figure 7).
525 It is also interesting to estimate the magnitude of inputs from the Eure watershed in the 1990s,
526 a period when very high Pb concentrations were recorded. Streamflow in the Eure River has
527 been near constant since 1971 (www.hydro.eaufrance.fr), assuming that 2017 corresponds to a
528 medium hydrological cycle in terms of hydro-sedimentary inputs. As such, theoretical flux
529 estimation for previous years using the SPM flux for the year 2017 and annual TMM
530 concentrations within sediment cores could prove insightful. The average Pb concentration
531 over 1992–1996 was 846 mg kg^{-1} (Figure 6; Table 3), which equates to an average flux of 95 t
532 y^{-1} , making the Eure watershed the main contributor of Pb to the Seine estuary (52%) (Figure
533 7). This confirms the river's classification as very high contamination by Meybeck et al.
534 (2004), and that the watershed has recently experienced major Pb contamination with little
535 national equivalency.

536

537 4.3. Sources of contamination

538

539 Similar temporal trends for Cr, Co, Ni, Cu, Zn, Ag, Cd (Figures 5A and 6) suggest that a
540 single anthropogenic source was responsible for the high levels over the 1960s–1970s. The
541 presence of Cd, Ni, Zn could be related to the activities and discharges of a saline batteries
542 factory. Within the Eure watershed there was a saline batteries factory (opened in the late
543 1930s), supplying most of the national market during the 1960s, resulting in very high
544 localised production. The factory was the subject of an increased administrative survey by a
545 national agency in the early 1970s (Agence Financière de Bassin “Seine-Normandie,” 1971).
546 This survey, coupled with the development of alkaline batteries (manufactured abroad), may
547 have caused a drop in production, resulting in a reduction in concentrations after the 1970s,
548 until the closure of the industrial site in 1994 (Gardes et al., 2020a).

549 The main source responsible for As release has not been defined but may be attributed to
550 different anthropogenic activities. This includes discharge from agricultural activities (e.g.,
551 wood preservative), industrial activities (glass and electronics industry, metal treatment,
552 ammunition manufacturing, production of dyes and colorants or metal smelters smelting) or
553 coal combustion (Reimann et al., 2009). But it must be noted that arsenical herbicides have
554 been forbidden in France since 1973; it is probable that it was one of the main sources in the
555 Eure watershed as the current concentrations, near the GB value, were reached after the
556 1970s.

557 Sources responsible for Pb contamination can be discriminated from Pb isotopes,
558 particularly in tri-isotopic diagrams in which these potential sources act as end-members (e.g.,
559 Cloquet et al., 2015). In the diagram $^{208}\text{Pb}/^{206}\text{Pb}$ versus $^{206}\text{Pb}/^{207}\text{Pb}$, the measurement within
560 the Seine Unit U2 ($^{208}\text{Pb}/^{206}\text{Pb} = 2.070$ and $^{206}\text{Pb}/^{207}\text{Pb} = 1.193$) was close to the points with a
561 natural (or pre-industrial) signature ($^{208}\text{Pb}/^{206}\text{Pb} = 2.053$ and $^{206}\text{Pb}/^{207}\text{Pb} = 1.2007$, Elbaz-
562 Poulichet et al., 1986; $^{208}\text{Pb}/^{206}\text{Pb} = 2.066$ and $^{206}\text{Pb}/^{207}\text{Pb} = 1.197$, Monna et al., 1997;
563 $^{208}\text{Pb}/^{206}\text{Pb} = 2.079$ and $^{206}\text{Pb}/^{207}\text{Pb} = 1.200$, Ferrand et al., 1999) (Figure 8A). Moreover, such
564 a high $^{206}\text{Pb}/^{207}\text{Pb}$ ratio has never been previously recorded in the Seine watershed (Ayrault et
565 al., 2012) with the exception of the upstream Yonne River where $^{206}\text{Pb}/^{207}\text{Pb}$ was
566 approximately 1.19 prior to the 1960s and after the 2000s. This reflects an absence of
567 anthropogenic Pb contamination (Ayrault et al., 2010). In terms of the Eure Unit U1, the
568 signature measured in 1965 ($^{208}\text{Pb}/^{206}\text{Pb} = 2.097$ et $^{206}\text{Pb}/^{207}\text{Pb} = 1.170$) showed a mix
569 between pre-industrial and industrial poles. It is possible to assess the relative contribution of
570 a source using the binary model, described for example by Komárek et al. (2008). Based on
571 the $^{206}\text{Pb}/^{207}\text{Pb}$ ratio proposed by Monna et al. (1997) as the average signature of French
572 industrial Pb ($^{206}\text{Pb}/^{207}\text{Pb} = 1.155$), the contribution of the unidentified industrial source, was
573 in the range 60–67%. This is dependent on the value used for the pre-industrial source,

574 between the Seine Unit from this study, and the values proposed by Elbaz-Poulichet et al.
575 (1986), Monna et al. (1997) and Ferrand et al. (1999). This shows that the contribution of
576 anthropogenic Pb was already significant during the 1960s in the Eure watershed, whereas Pb
577 concentrations recorded in sediment cores at the same time were not high and did not exhibit
578 an increasing trend (Figure 5A). However, the estimation of this contribution does not
579 consider a possible existing contribution from other sources such as coal use (e.g., coal power
580 plant, coal combustion), which is also a source of Pb. Notably, the isotope signature recorded
581 in 1965 was close to the isotope signatures of Pb from coal use (Cloquet et al., 2006; Elbaz-
582 Poulichet et al., 2011). Although it is unlikely that there existed only a single source emitting
583 Pb during the 1960s. This 1960s signature was close to the European Standard Lead Pollution
584 (ESLP) line defined by Haack et al. (2002, 2003) from atmospheric Pb deposition across
585 Europe, confirming the presence of anthropogenic Pb in this sample. More recent
586 contamination signatures (1995, 1997, 2002 and 2012) were located between the industrial
587 and leaded petrol poles (defined from data from Monna et al. (1997), Véron et al. (1999) and
588 Cloquet et al. (2015)). These were aligned with the industrial Pb line also defined by Haack et
589 al. (2002, 2003) from industrial equipment, exhaust pipes and several major ore deposits. As
590 such, it is possible to envisage a mixture between these two poles to understand the signatures
591 obtained recently in the Eure watershed. Figure 8B shows that these signatures, in particular
592 that of 1995, were close to a Pb smelting signature defined in northern France from aerosols
593 ($n = 2$; $^{208}\text{Pb}/^{206}\text{Pb} = 2.1269 \pm 0.0008$ et $^{206}\text{Pb}/^{207}\text{Pb} = 1.1330 \pm 0.0009$ (Véron et al., 1999)),
594 or dust from a Pb-Zn smelting plant ($n = 2$; $^{208}\text{Pb}/^{206}\text{Pb} = 2.124 \pm 0.002$ et $^{206}\text{Pb}/^{207}\text{Pb} =$
595 1.1289 ± 0.0023 (Cloquet et al., 2006)) (not shown in Figure 8B). However, these authors do
596 not consider contributions from leaded gasoline. Therefore, the signature recorded here for
597 these four points was the result of an anthropogenic Pb input, the partial source of which
598 could be the same as that recorded by the signature measured in 1965. The difference in

599 signature between 1965 and more recent signatures may also be attributable to an increase in a
600 major anthropogenic source not yet identified but unrelated to coal (indicated by increases in
601 Pb concentrations as seen in the sediment cores). There is an anthropogenic source of Pb in
602 the Eure watershed related to industrial activities that commenced in the 1960s and increased
603 from the 1990s. Chiffoleau et al. (2012) used a sediment core sampled in the Seine estuary to
604 demonstrate that there was a single anthropogenic source which accounts for the variations in
605 the $^{206}\text{Pb}/^{207}\text{Pb}$ ratio in the estuary since 1975. Between 1975 and 1985 the variations in this
606 ratio are explained by a mixture between intra-estuarine phosphogypsum discharges and an
607 unknown anthropogenic source. Post-1985 the variations may be attributed to a mixture
608 between a natural source and this same unknown anthropogenic source. The isotopic signature
609 of this source ($^{208}\text{Pb}/^{206}\text{Pb} = 2.132$ et $^{206}\text{Pb}/^{207}\text{Pb} = 1.13$) was isolated by Chiffoleau et al.
610 (2012) and Figure 8B shows that it is close to the anthropogenic signature recorded by the
611 Eure River sediments, indicating that it is likely the source comes from the Eure River. Based
612 on the SPM sampled in the Eure River in March and September 2009 (and of dissolved Pb
613 (Pb_d) measurements), Chiffoleau et al. (2012) estimated a low $^{206}\text{Pb}/^{207}\text{Pb}$ ratio, in the range
614 1.12–1.14, consistent with ratios from our study (Figure 8B). From a sampling campaign
615 conducted in September 2011, Chiffoleau et al. (2012) found an increase in Pb_d and a
616 $^{206}\text{Pb}/^{207}\text{Pb}$ ratio of about 1.13 downstream of the city of Dreux (and a $^{206}\text{Pb}/^{207}\text{Pb}$ ratio greater
617 than 1.14 upstream). Assuming the mixture of natural and anthropogenic sources, the authors
618 estimated that the additional anthropogenic source had a $^{206}\text{Pb}/^{207}\text{Pb}$ signature of
619 approximately 1.12. A cathode-ray tube (CRT) factory began operation in Dreux in 1956 and
620 a second factory, specialising in the assembly of CRT TVs and the manufacture of electrical
621 circuits, opened in 1974 at the same industrial site. Chiffoleau et al. (2012) hypothesised that
622 the CRT factory represented this unknown Pb source. CRT may contain up to 3 kg of Pb
623 (Tsydenova and Bengtsson, 2011). This factory, as well as the CRT TVs assembly factory,

624 was purchased in the early 1990s to boost the economy (and thus increase CRT production)
625 prior to closing in 2006 and 2010 for the CRT factory and CRT TVs assembly factory,
626 respectively. In 2001, Pb discharge to water from the industrial site was ranked among the
627 highest in Europe by the European Environment Agency (E-PRTR, 2006). Increases in Pb_p
628 within sediment cores since the 1990s, as well as isotope signatures measured in 1995, 1997
629 and 2002, reflect the economic recovery initiated by this industry. However, the high
630 concentrations measured from the end of the 2000s in the sediment cores, and the isotopic
631 signature estimated in 2012, demonstrate that anthropogenic Pb inputs are still present in the
632 Eure watershed despite the cessation of industrial activities. These inputs are sufficiently high
633 to modify the ²⁰⁶Pb/²⁰⁷Pb ratio in the SPM of the Seine estuary as shown by Chiffolleau et al.
634 (2012).

635

636 **5. Conclusions**

637

638 This study of sediment cores has revealed that the lower reaches of the Eure watershed have
639 been subject to significant anthropogenic pressures since the 1940s, at comparable or higher
640 levels, than those experienced by other French watersheds during the twentieth century. The
641 temporal trends of TMM concentrations have shown strong anthropogenic impacts, mainly of
642 industrial origin during the 1960s and 1970s. A general trend towards a decrease in impacts
643 was emerging at the end of the twentieth century, as in the majority of French river
644 watersheds. However, an additional source, potentially of industrial origin, was responsible
645 for high Pb discharges that heavily contaminated sediments of the Eure River. It had a
646 signature found in sediments of the Seine estuary, that had already been heavily impacted by
647 inputs from the fluvial part of Seine River, one of the most anthropized catchments in Europe.
648 The similarity between the levels of TMM in the most recent sedimentary deposits and on the

649 SPM showed that the sedimentary records were representative of SPM transfers, and that the
650 footprint of industrial contamination was still present despite the cessation of the activities
651 responsible for the discharges. This footprint reflects the existence of permanent
652 anthropogenic baseline within the river, resulting from the erosion of contaminated soils and
653 sediments stored in the river and remobilised during floods and/or landscaping projects. As a
654 result, the current flux in TMM to the Seine estuary remain significant despite the cessation or
655 drastic reduction of discharges from anthropogenic activities. Based on the estimation of past
656 theoretical flows, it has been shown in the case of Pb that the Eure watershed could exceed
657 contributions from the Seine watershed, making the former the main contributor of Pb to the
658 Seine estuary during the 1990s.

659

660 **Reference data**

661 The dataset is available at <https://doi.org/10.1594/PANGAEA.912843> (Gardes et al., 2020b)
662 and at <https://doi.org/10.1594/PANGAEA.911102> (Gardes et al., 2020c).

663

664 **Acknowledgements**

665 This work is part of the OSS 276 project, financially supported by the Seine-Normandie
666 Water Agency (France). This work is support by the CNRS toward EC2CO grant (Avant-
667 Seine project). Gardes Th. grant was funded by the Region Normandie, which supports the
668 scientific consortium SCALE UMR CNRS 3730. CNRS also supports the French national
669 cyber-Repository (<https://www.cybercarotheque.fr/>) which is a portal for metadata associated
670 with marine, lake/river sediment cores stored in French laboratories. This project was initiated
671 by CLIMCOR project (<http://climcor-equipex.dt.insu.cnrs.fr/>).

672 Our paper is a contribution to ROZA-LTER-fr project : Retro-Observatory of sedimentary
673 Archive from French LTER (<http://ccwbvps18.in2p3.fr/maps/visualiseur-coyoxhup#project>)
674 which is a portal for data associated with marine, lake sediment cores stored in LTER French
675 laboratories.

676 Authors sincerely thank the “Parc Naturel Régional du Perche” for allowing the access at the
677 ponds and Aurélie Tran Van Loc for her participation at the coring session.

678 Authors also thank Romain Levaillant and Michel Simon (M2C laboratory) for their
679 participation in the field sampling (coring sessions, TIMS deployment).

680

681 **References**

682

683 Ackermann, F., 1980. A procedure for correcting the grain size effect in heavy metal analyses
684 of estuarine and coastal sediments. *Environ. Technol. Lett.* 1, 518–527.

685 <https://doi.org/10.1080/09593338009384008>

686 Agence Financière de Bassin “Seine-Normandie,” 1971. Délibération n°71-16 du 21 Octobre
687 1971 désignant les entreprises industrielles soumises à la mesure pour le calcul de leur
688 redevance pollution.

689 Appleby, P.G., Richardson, N., Nolan, P.J., 1991. ²⁴¹Am dating of lake sediments.

690 *Hydrobiologia* 214, 35–42. <https://doi.org/10.1007/BF00050929>

691 Audry, S., Blanc, G., Schäfer, J., Chaillou, G., Robert, S., 2006. Early diagenesis of trace
692 metals (Cd, Cu, Co, Ni, U, Mo, and V) in the freshwater reaches of a macrotidal
693 estuary. *Geochim. Cosmochim. Acta* 70, 2264–2282.

694 <https://doi.org/10.1016/j.gca.2006.02.001>

695 Audry, S., Schäfer, J., Blanc, G., Jouanneau, J.-M., 2004. Fifty-year sedimentary record of
696 heavy metal pollution (Cd, Zn, Cu, Pb) in the Lot River reservoirs (France). *Environ.*
697 *Pollut.* 132, 413–426. <https://doi.org/10.1016/j.envpol.2004.05.025>

698 Ayrault, S., Lorgeoux, C., Moilleron, R., Lherm, D., Tassin, B., Bonté, P., Roy-Barman, M.,
699 Le, M.-F., Lefèvre, I., Priadi, C., Evrard, O., Bordier, L., Mouchel, J.-M., Eurin, J.,
700 Tamtam, F., Dinh, T., Boust, D., Vrel, A., 2010. Archives sédimentaires, empreintes
701 des micropolluants sur le bassin de la Seine sur 80 ans. *PIREN-Seine Rapp. Act.* 2010
702 34.

703 Ayrault, S., Roy-Barman, M., Le Cloarec, M.-F., Priadi, C.R., Bonté, P., Göpel, C., 2012.

704 Lead contamination of the Seine River, France: Geochemical implications of a
705 historical perspective. *Chemosphere* 87, 902–910.

706 <https://doi.org/10.1016/j.chemosphere.2012.01.043>

707 Bábek, O., Grygar, T.M., Faměra, M., Hron, K., Nováková, T., Sedláček, J., 2015.

708 Geochemical background in polluted river sediments: How to separate the effects of
709 sediment provenance and grain size with statistical rigour? *CATENA* 135, 240–253.

710 <https://doi.org/10.1016/j.catena.2015.07.003>

711 Bajard, M., Etienne, D., Quinsac, S., Dambrine, E., Sabatier, P., Frossard, V., Gaillard, J.,

712 Develle, A.-L., Poulenard, J., Arnaud, F., Dorioz, J.-M., 2018. Legacy of early
713 anthropogenic effects on recent lake eutrophication (Lake Bénit, northern French

714 Alps). *Anthropocene* 24, 72–87. <https://doi.org/10.1016/j.ancene.2018.11.005>

715 Bruel, R., Sabatier, P., 2020. serac: a R package for ShortlivEd RADionuclide Chronology of
716 recent sediment cores. *EarthArXiv* 1–38. <https://doi.org/10.31223/osf.io/f4yma>

717 Brüggmann, L., 1995. Metals in sediments and suspended matter of the river Elbe. *Sci. Total*
718 *Environ.* 159, 53–65. [https://doi.org/10.1016/0048-9697\(94\)04252-1](https://doi.org/10.1016/0048-9697(94)04252-1)

719 Callender, E., 2000. Geochemical effects of rapid sedimentation in aquatic systems: minimal
720 diagenesis and the preservation of historical metal signatures. *J. Paleolimnol.* 23, 243–
721 260. <https://doi.org/10.1023/A:1008114630756>

722 Chiaradia, M., Gallay, A., Todt, W., 2003. Different contamination styles of prehistoric
723 human teeth at a Swiss necropolis (Sion, Valais) inferred from lead and strontium
724 isotopes. *Appl. Geochem.* 18, 353–370. [https://doi.org/10.1016/S0883-](https://doi.org/10.1016/S0883-2927(02)00072-0)

725 [2927\(02\)00072-0](https://doi.org/10.1016/S0883-2927(02)00072-0)

- 726 Chiffolleau, J.-F., Sonke, J.E., Auger, D., Bretaudeau, J., Joguet, T., Larrieu, M., Laffont, L.,
727 Prunier, J., Rozuel, E., Zouiten, C., 2012. Etude de la signature isotopique des métaux
728 dans l'estuaire de la Seine. Une information essentielle pour le traçage et la
729 discrimination des sources et processus.
- 730 Cloquet, C., Carignan, J., Libourel, G., 2006a. Atmospheric pollutant dispersion around an
731 urban area using trace metal concentrations and Pb isotopic compositions in epiphytic
732 lichens. *Atmos. Environ.* 40, 574–587. <https://doi.org/10.1016/j.atmosenv.2005.09.073>
- 733 Cloquet, C., Carignan, J., Libourel, G., Sterckeman, T., Perdrix, E., 2006b. Tracing Source
734 Pollution in Soils Using Cadmium and Lead Isotopes. *Environ. Sci. Technol.* 40,
735 2525–2530. <https://doi.org/10.1021/es052232+>
- 736 Cloquet, C., Estrade, N., Carignan, J., 2015. Ten years of elemental atmospheric metal fallout
737 and Pb isotopic composition monitoring using lichens in northeastern France.
738 *Comptes Rendus Geosci., Geochemical and isotopic record of anthropogenic activities*
739 (Part 1) 347, 257–266. <https://doi.org/10.1016/j.crte.2015.04.003>
- 740 Copard, Y., Di-Giovanni, C., Martaud, T., Albéric, P., Olivier, J.-E., 2006. Using Rock-Eval 6
741 pyrolysis for tracking fossil organic carbon in modern environments: implications for
742 the roles of erosion and weathering. *Earth Surf. Process. Landf.* 31, 135–153.
743 <https://doi.org/10.1002/esp.1319>
- 744 Coynel, A., Gorse, L., Curti, C., Schafer, J., Grosbois, C., Morelli, G., Ducassou, E., Blanc,
745 G., Maillet, G.M., Mojtahid, M., 2016. Spatial distribution of trace elements in the
746 surface sediments of a major European estuary (Loire Estuary, France): Source
747 identification and evaluation of anthropogenic contribution. *J. Sea Res., Recent and*
748 *past sedimentary, biogeochemical and benthic ecosystem evolution of the Loire*
749 *Estuary (Western France)* 118, 77–91. <https://doi.org/10.1016/j.seares.2016.08.005>
- 750 Coynel, A., Schäfer, J., Blanc, G., Bossy, C., 2007. Scenario of particulate trace metal and
751 metalloid transport during a major flood event inferred from transient geochemical
752 signals. *Appl. Geochem.* 22, 821–836.
753 <https://doi.org/10.1016/j.apgeochem.2006.10.004>
- 754 Daskalakis, K.D., O'Connor, T.P., 1995. Normalization and Elemental Sediment
755 Contamination in the Coastal United States. *Environ. Sci. Technol.* 29, 470–477.
756 <https://doi.org/10.1021/es00002a024>
- 757 Dhivert, E., Grosbois, C., Courtin-Nomade, A., Bourrain, X., Desmet, M., 2016. Dynamics of
758 metallic contaminants at a basin scale — Spatial and temporal reconstruction from
759 four sediment cores (Loire fluvial system, France). *Sci. Total Environ.* 541, 1504–
760 1515. <https://doi.org/10.1016/j.scitotenv.2015.09.146>
- 761 Duan, D., Ran, Y., Cheng, H., Chen, J., Wan, G., 2014. Contamination trends of trace metals
762 and coupling with algal productivity in sediment cores in Pearl River Delta, South
763 China. *Chemosphere* 103, 35–43. <https://doi.org/10.1016/j.chemosphere.2013.11.011>
- 764 Elbaz-Poulichet, F., Dezileau, L., Freydier, R., Cossa, D., Sabatier, P., 2011. A 3500-Year
765 Record of Hg and Pb Contamination in a Mediterranean Sedimentary Archive (The
766 Pierre Blanche Lagoon, France). *Environ. Sci. Technol.* 45, 8642–8647.
767 <https://doi.org/10.1021/es2004599>
- 768 Elbaz-Poulichet, F., Guédron, S., Anne-Lise, D., Freydier, R., Perrot, V., Rossi, M., Piot, C.,
769 Delpoux, S., Sabatier, P., 2020. A 10,000-year record of trace metal and metalloid
770 (Cu, Hg, Sb, Pb) deposition in a western Alpine lake (Lake Robert, France):
771 Deciphering local and regional mining contamination. *Quat. Sci. Rev.* 228, 106076.
772 <https://doi.org/10.1016/j.quascirev.2019.106076>
- 773 Elbaz-Poulichet, F., Holliger, P., Martin, J.M., Petit, D., 1986. Stable lead isotopes ratios in
774 major french rivers and estuaries. *Sci. Total Environ.* 54, 61–76.
775 [https://doi.org/10.1016/0048-9697\(86\)90256-1](https://doi.org/10.1016/0048-9697(86)90256-1)

776 E-PRTR [WWW Document], 2006. . Eur. Environ. Agency. URL
777 [https://www.eea.europa.eu/data-and-maps/data/member-states-reporting-art-7-under-](https://www.eea.europa.eu/data-and-maps/data/member-states-reporting-art-7-under-the-european-pollutant-release-and-transfer-register-e-prtr-regulation-18)
778 [the-european-pollutant-release-and-transfer-register-e-prtr-regulation-18](https://www.eea.europa.eu/data-and-maps/data/member-states-reporting-art-7-under-the-european-pollutant-release-and-transfer-register-e-prtr-regulation-18) (accessed
779 6.4.19).

780 Ferrand, E., Eyrolle, F., Radakovitch, O., Provansal, M., Dufour, S., Vella, C., Raccasi, G.,
781 Gurriaran, R., 2012. Historical levels of heavy metals and artificial radionuclides
782 reconstructed from overbank sediment records in lower Rhône River (South-East
783 France). *Geochim. Cosmochim. Acta, Environmental Records of Anthropogenic*
784 *Impacts* 82, 163–182. <https://doi.org/10.1016/j.gca.2011.11.023>

785 Ferrand, J.-L., Hamelin, B., Monaco, A., 1999. Isotopic tracing of anthropogenic Pb
786 inventories and sedimentary fluxes in the Gulf of Lions (NW Mediterranean sea).
787 *Cont. Shelf Res.* 19, 23–47. [https://doi.org/10.1016/S0278-4343\(98\)00070-3](https://doi.org/10.1016/S0278-4343(98)00070-3)

788 Foster, I.D.L., Charlesworth, S.M., 1996. Heavy metals in the hydrological cycle: Trends and
789 explanation. *Hydrol. Process.* 10, 227–261. [https://doi.org/10.1002/\(SICI\)1099-](https://doi.org/10.1002/(SICI)1099-1085(199602)10:2<227::AID-HYP357>3.0.CO;2-X)
790 [1085\(199602\)10:2<227::AID-HYP357>3.0.CO;2-X](https://doi.org/10.1002/(SICI)1099-1085(199602)10:2<227::AID-HYP357>3.0.CO;2-X)

791 Gale, N.H., 1996. A new method for extracting and purifying lead from difficult matrices for
792 isotopic analysis. *Anal. Chim. Acta* 332, 15–21. [https://doi.org/10.1016/0003-](https://doi.org/10.1016/0003-2670(96)00207-3)
793 [2670\(96\)00207-3](https://doi.org/10.1016/0003-2670(96)00207-3)

794 Gardes, T., Debret, M., Copard, Y., Patault, E., Winiarski, T., Develle, A.-L., Sabatier, P.,
795 Dendievel, A.-M., Mourier, B., Marcotte, S., Leroy, B., Portet-Koltalo, F., 2020a.
796 Reconstruction of anthropogenic activities in legacy sediments from the Eure River, a
797 major tributary of the Seine Estuary (France). *CATENA* 190, 104513.
798 <https://doi.org/10.1016/j.catena.2020.104513>

799 Gardes, T., Debret, M., Copard, Y., Coynel, A., Deloffre, J., Fournier, M., Revillon, S.,
800 Nizou, J., Develle, A.-L., Sabatier, P., Marcotte, S., Patault, E., Faivre, Q., Portet-
801 Koltalo, F., 2020b. Trace metals and metalloid elements in sediment cores (1940s-
802 2017) and suspended particulate matter (2017-2018) from the Eure River, France.
803 *PANGAEA*. <https://doi.org/10.1594/PANGAEA.912843>

804 Gardes, T., Debret, M., Copard, Y., Patault, E., Winiarski, T., Develle, A.-L., Sabatier, P.,
805 Dendievel, A.-M., Mourier, B., Marcotte, S., Leroy, B., Portet-Koltalo, F., 2020c.
806 Reconstruction of anthropogenic activities in sediments cores from the Eure River.
807 *PANGAEA*. <https://doi.org/10.1594/PANGAEA.911102>

808 Gascón Díez, E., Corella, J.P., Adatte, T., Thevenon, F., Loizeau, J.-L., 2017. High-resolution
809 reconstruction of the 20th century history of trace metals, major elements, and organic
810 matter in sediments in a contaminated area of Lake Geneva, Switzerland. *Appl.*
811 *Geochem.* 78, 1–11. <https://doi.org/10.1016/j.apgeochem.2016.12.007>

812 Goldberg, E.L., 1963. Geochronology with ²¹⁰Pb. *Radioact. Dating Int. At. Energy Agency*
813 121–131.

814 Grosbois, C., Meybeck, M., Lestel, L., Lefèvre, I., Moatar, F., 2012. Severe and contrasted
815 polymetallic contamination patterns (1900–2009) in the Loire River sediments
816 (France). *Sci. Total Environ.* 435–436, 290–305.
817 <https://doi.org/10.1016/j.scitotenv.2012.06.056>

818 Grousset, F.E., Jouanneau, J.M., Castaing, P., Lavaux, G., Latouche, C., 1999. A 70 year
819 Record of Contamination from Industrial Activity Along the Garonne River and its
820 Tributaries (SW France). *Estuar. Coast. Shelf Sci.* 48, 401–414.
821 <https://doi.org/10.1006/ecss.1998.0435>

822 Haack, U.K., Gutsche, F.H., Plessow, K., Heinrichs, H., 2002. On the Isotopic Composition
823 of Pb in Cloud Waters in Central Germany. A Source Discrimination Study. *Water.*
824 *Air. Soil Pollut.* 139, 261–288. <https://doi.org/10.1023/A:1015864103834>

- 825 Haack, U.K., Heinrichs, H., Gutsche, F.H., Plessow, K., 2003. The Isotopic Composition of
826 Anthropogenic Pb in Soil Profiles of Northern Germany: Evidence for Pollutant Pb
827 from a Continent-wide Mixing System. *Water, Air, Soil Pollut.* 150, 113–134.
828 <https://doi.org/10.1023/A:1026142501593>
- 829 He, Q., Walling, D.E., 1996. Interpreting particle size effects in the adsorption of ¹³⁷Cs and
830 unsupported ²¹⁰Pb by mineral soils and sediments. *J. Environ. Radioact.* 30, 117–137.
831 [https://doi.org/10.1016/0265-931X\(96\)89275-7](https://doi.org/10.1016/0265-931X(96)89275-7)
- 832 Hennekam, R., Sweere, T., Tjallingii, R., de Lange, G.J., Reichart, G.-J., 2019. Trace metal
833 analysis of sediment cores using a novel X-ray fluorescence core scanning method.
834 *Quat. Int., Advances in Data Quantification and Application of high resolution XRF*
835 *Core Scanners* 514, 55–67. <https://doi.org/10.1016/j.quaint.2018.10.018>
- 836 Horowitz, A.J., Elrick, K.A., 1987. The relation of stream sediment surface area, grain size
837 and composition to trace element chemistry. *Appl. Geochem.* 2, 437–451.
838 [https://doi.org/10.1016/0883-2927\(87\)90027-8](https://doi.org/10.1016/0883-2927(87)90027-8)
- 839 Horowitz, A.J., Meybeck, M., Idlafkih, Z., Biger, E., 1999. Variations in trace element
840 geochemistry in the Seine River Basin based on floodplain deposits and bed
841 sediments. *Hydrol. Process.* 13, 1329–1340. [https://doi.org/10.1002/\(SICI\)1099-1085\(19990630\)13:9<1329::AID-HYP811>3.0.CO;2-H](https://doi.org/10.1002/(SICI)1099-1085(19990630)13:9<1329::AID-HYP811>3.0.CO;2-H)
- 842 Komárek, M., Ettler, V., Chrastný, V., Mihaljevič, M., 2008. Lead isotopes in environmental
843 sciences: A review. *Environ. Int.* 34, 562–577.
844 <https://doi.org/10.1016/j.envint.2007.10.005>
- 845 Krishnaswamy, S., Lal, D., Martin, J.M., Meybeck, M., 1971. Geochronology of lake
846 sediments. *Earth Planet. Sci. Lett.* 11, 407–414. [https://doi.org/10.1016/0012-821X\(71\)90202-0](https://doi.org/10.1016/0012-821X(71)90202-0)
- 847
848
- 849 Laignel, B., Quesnel, F., Lecoustumer, M.-N., Meyer, R., 1998. Variabilité du cortège
850 argileux des formations résiduelles à silex de l’Ouest du bassin de Paris. *Comptes*
851 *Rendus Académie Sci. - Ser. IIA - Earth Planet. Sci.* 326, 467–472.
852 [https://doi.org/10.1016/S1251-8050\(98\)80072-4](https://doi.org/10.1016/S1251-8050(98)80072-4)
- 853 Lancelot, L., Schäfer, J., Bossy, C., Coynel, A., Larrose, A., Masson, M., Blanc, G., 2011a.
854 Silver fluxes to the Gironde Estuary – Eleven years (1999–2009) of monitoring at the
855 watershed scale. *Appl. Geochem.* 26, 797–808.
856 <https://doi.org/10.1016/j.apgeochem.2011.02.001>
- 857 Lancelot, L., Schäfer, J., Chiffolleau, J.-F., Blanc, G., Auger, D., Renault, S., Baudrimont,
858 M., Audry, S., 2011b. Long-term records of cadmium and silver contamination in
859 sediments and oysters from the Gironde fluvial–estuarine continuum – Evidence of
860 changing silver sources. *Chemosphere* 85, 1299–1305.
861 <https://doi.org/10.1016/j.chemosphere.2011.07.036>
- 862 Larrose, A., Coynel, A., Schäfer, J., Blanc, G., Massé, L., Maneux, E., 2010. Assessing the
863 current state of the Gironde Estuary by mapping priority contaminant distribution and
864 risk potential in surface sediment. *Appl. Geochem.* 25, 1912–1923.
865 <https://doi.org/10.1016/j.apgeochem.2010.10.007>
- 866 Le Cloarec, M.-F., Bonte, P.H., Lestel, L., Lefèvre, I., Ayrault, S., 2011. Sedimentary record
867 of metal contamination in the Seine River during the last century. *Phys. Chem. Earth*
868 *Parts ABC, Man and River Systems: From pressures to physical, chemical and*
869 *ecological status* 36, 515–529. <https://doi.org/10.1016/j.pce.2009.02.003>
- 870 Lepland, Aivo, Andersen, T.J., Lepland, Aave, Arp, H.P.H., Alve, E., Breedveld, G.D.,
871 Rindby, A., 2010. Sedimentation and chronology of heavy metal pollution in Oslo
872 harbor, Norway. *Mar. Pollut. Bull.* 60, 1512–1522.
873 <https://doi.org/10.1016/j.marpolbul.2010.04.017>

- 874 Masson, M., Blanc, G., Schäfer, J., Parlanti, E., Le Coustumer, P., 2011. Copper addition by
875 organic matter degradation in the freshwater reaches of a turbid estuary. *Sci. Total*
876 *Environ.* 409, 1539–1549. <https://doi.org/10.1016/j.scitotenv.2011.01.022>
- 877 Meybeck, M., Horowitz, A.J., Grosbois, C., 2004. The geochemistry of Seine River Basin
878 particulate matter: distribution of an integrated metal pollution index. *Sci. Total*
879 *Environ.* 328, 219–236. <https://doi.org/10.1016/j.scitotenv.2004.01.024>
- 880 Monna, F., Lancelot, J., Croudace, I.W., Cundy, A.B., Lewis, J.T., 1997. Pb Isotopic
881 Composition of Airborne Particulate Material from France and the Southern United
882 Kingdom: Implications for Pb Pollution Sources in Urban Areas. *Environ. Sci.*
883 *Technol.* 31, 2277–2286. <https://doi.org/10.1021/es960870+>
- 884 Petit, J.C.J., Schäfer, J., Coynel, A., Blanc, G., Deycard, V.N., Derriennic, H., Lancelot, L.,
885 Dutruch, L., Bossy, C., Mattielli, N., 2013. Anthropogenic sources and
886 biogeochemical reactivity of particulate and dissolved Cu isotopes in the turbidity
887 gradient of the Garonne River (France). *Chem. Geol.* 359, 125–135.
888 <https://doi.org/10.1016/j.chemgeo.2013.09.019>
- 889 Phillips, J.M., Russell, M.A., Walling, D.E., 2000. Time-integrated sampling of fluvial
890 suspended sediment: a simple methodology for small catchments. *Hydrol. Process.* 14,
891 2589–2602. [https://doi.org/10.1002/1099-1085\(20001015\)14:14<2589::AID-
892 HYP94>3.0.CO;2-D](https://doi.org/10.1002/1099-1085(20001015)14:14<2589::AID-HYP94>3.0.CO;2-D)
- 893 Quesnel, F., 1997. Digital mapping in regolith geology. *Cartographie numérique en géologie*
894 *de surface. Application aux altérites à silex de l'Ouest du bassin de Paris (Theses).*
895 Université de Rouen.
- 896 Reimann, C., Matschullat, J., Birke, M., Salminen, R., 2009. Arsenic distribution in the
897 environment: The effects of scale. *Appl. Geochem.* 24, 1147–1167.
898 <https://doi.org/10.1016/j.apgeochem.2009.03.013>
- 899 Reimer, P.J., Bard, E., Bayliss, A., Beck, J.W., Blackwell, P.G., Ramsey, C.B., Buck, C.E.,
900 Cheng, H., Edwards, R.L., Friedrich, M., Grootes, P.M., Guilderson, T.P., Haffidason,
901 H., Hajdas, I., Hatté, C., Heaton, T.J., Hoffmann, D.L., Hogg, A.G., Hughen, K.A.,
902 Kaiser, K.F., Kromer, B., Manning, S.W., Niu, M., Reimer, R.W., Richards, D.A.,
903 Scott, E.M., Southon, J.R., Staff, R.A., Turney, C.S.M., Plicht, J. van der, 2013.
904 IntCal13 and Marine13 Radiocarbon Age Calibration Curves 0–50,000 Years cal BP.
905 *Radiocarbon* 55, 1869–1887. https://doi.org/10.2458/azu_js_rc.55.16947
- 906 Richter, T.O., Gaast, S. van der, Koster, B., Vaars, A., Gieles, R., Stigter, H.C. de, Haas,
907 H.D., Weering, T.C.E. van, 2006. The Avaatech XRF Core Scanner: technical
908 description and applications to NE Atlantic sediments. *Geol. Soc. Lond. Spec. Publ.*
909 267, 39–50. <https://doi.org/10.1144/GSL.SP.2006.267.01.03>
- 910 Robbins, J.A., Edgington, D.N., 1975. Determination of recent sedimentation rates in Lake
911 Michigan using Pb-210 and Cs-137. *Geochim. Cosmochim. Acta* 39, 285–304.
912 [https://doi.org/10.1016/0016-7037\(75\)90198-2](https://doi.org/10.1016/0016-7037(75)90198-2)
- 913 Russell, M.A., Walling, D.E., Hodgkinson, R.A., 2000. Appraisal of a simple sampling device
914 for collecting time-integrated fluvial suspended sediment samples. The role of erosion
915 and sediment transport in nutrient and contaminant transfer (Proceedings Waterloo
916 Symposium, 2000). *IAHS Publ.* 263, 119–127.
- 917 Sabatier, P., Poulénard, J., Fanget, B., Reyss, J.-L., Develle, A.-L., Wilhelm, B., Ployon, E.,
918 Pignol, C., Naffrechoux, E., Dorioz, J.-M., Montuelle, B., Arnaud, F., 2014. Long-
919 term relationships among pesticide applications, mobility, and soil erosion in a
920 vineyard watershed. *Proc. Natl. Acad. Sci. U. S. A.* 111, 15647–15652.
921 <https://doi.org/10.1073/pnas.1411512111>
- 922 Salomons, W., Forstner, U., 1984. Metals in the hydrocycle. *Met. Hydrocycle.*

- 923 Thévenot, D., Moilleron, R., Lestel, L., Gromaire, M.C., Rocher, V., Cambier, P., Bonté, P.,
924 Colin, J.-L., de Ponteves, C., Meybeck, M., 2007. Critical budget of metal sources
925 and pathways in the Seine River basin (1994–2003) for Cd, Cr, Cu, Hg, Ni, Pb and Zn.
926 *Sci. Total Environ.* 375.
- 927 Tseng, C.M., Amouroux, D., Abril, G., Tessier, E., Etcheber, H., Donard, O.F.X., 2001.
928 Speciation of Mercury in a Fluid Mud Profile of a Highly Turbid Macrotidal Estuary
929 (Gironde, France). *Environ. Sci. Technol.* 35, 2627–2633.
930 <https://doi.org/10.1021/es001750b>
- 931 Tsydenova, O., Bengtsson, M., 2011. Chemical hazards associated with treatment of waste
932 electrical and electronic equipment. *Waste Manag.* 31, 45–58.
933 <https://doi.org/10.1016/j.wasman.2010.08.014>
- 934 Van Calsteren, P., Thomas, L., 2006. Uranium-series dating applications in natural
935 environmental science. *Earth-Sci. Rev., ISOTopes in PALaeoenvironmental*
936 *reconstruction (ISOPAL)* 75, 155–175. <https://doi.org/10.1016/j.earscirev.2005.09.001>
- 937 Véron, A., Flament, P., Bertho, M.L., Alleman, L., Flegel, R., Hamelin, B., 1999. Isotopic
938 evidence of pollutant lead sources in Northwestern France. *Atmos. Environ.* 33, 3377–
939 3388. [https://doi.org/10.1016/S1352-2310\(98\)00376-8](https://doi.org/10.1016/S1352-2310(98)00376-8)
- 940 Vrel, A., 2012. Reconstitution de l’historique des apports en radionucléides et contaminants
941 métalliques à l’estuaire fluvial de la Seine par l’analyse de leur enregistrement
942 sédimentaire.
- 943 Wedepohl, K.H., 1995. The composition of the continental crust. *Geochim. Cosmochim. Acta*
944 59, 1217–1232. [https://doi.org/10.1016/0016-7037\(95\)00038-2](https://doi.org/10.1016/0016-7037(95)00038-2)
- 945 White, W.M., Albarède, F., Télouk, P., 2000. High-precision analysis of Pb isotope ratios by
946 multi-collector ICP-MS. *Chem. Geol.* 167, 257–270. [https://doi.org/10.1016/S0009-
947 2541\(99\)00182-5](https://doi.org/10.1016/S0009-2541(99)00182-5)
- 948

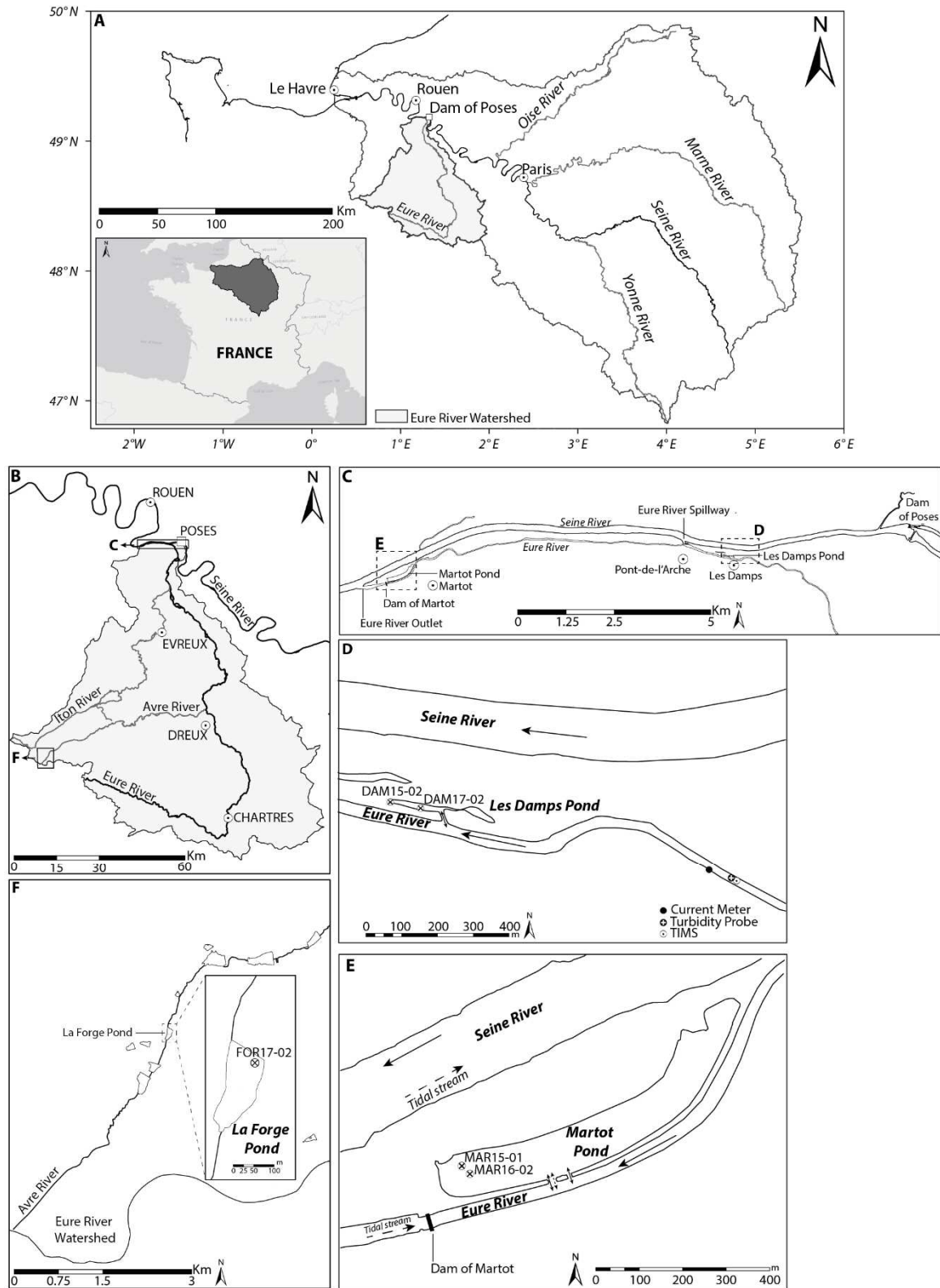


Figure 1. A. The Seine River Watershed; B. The Eure River Watershed; C. Study Area; D. Sediment core locations in the Les Damps Pond and current meter, turbidity probe and TIMS locations; E. Sediment core locations in the Martot Pond and F. Sediment core location in the La Forge Pond.

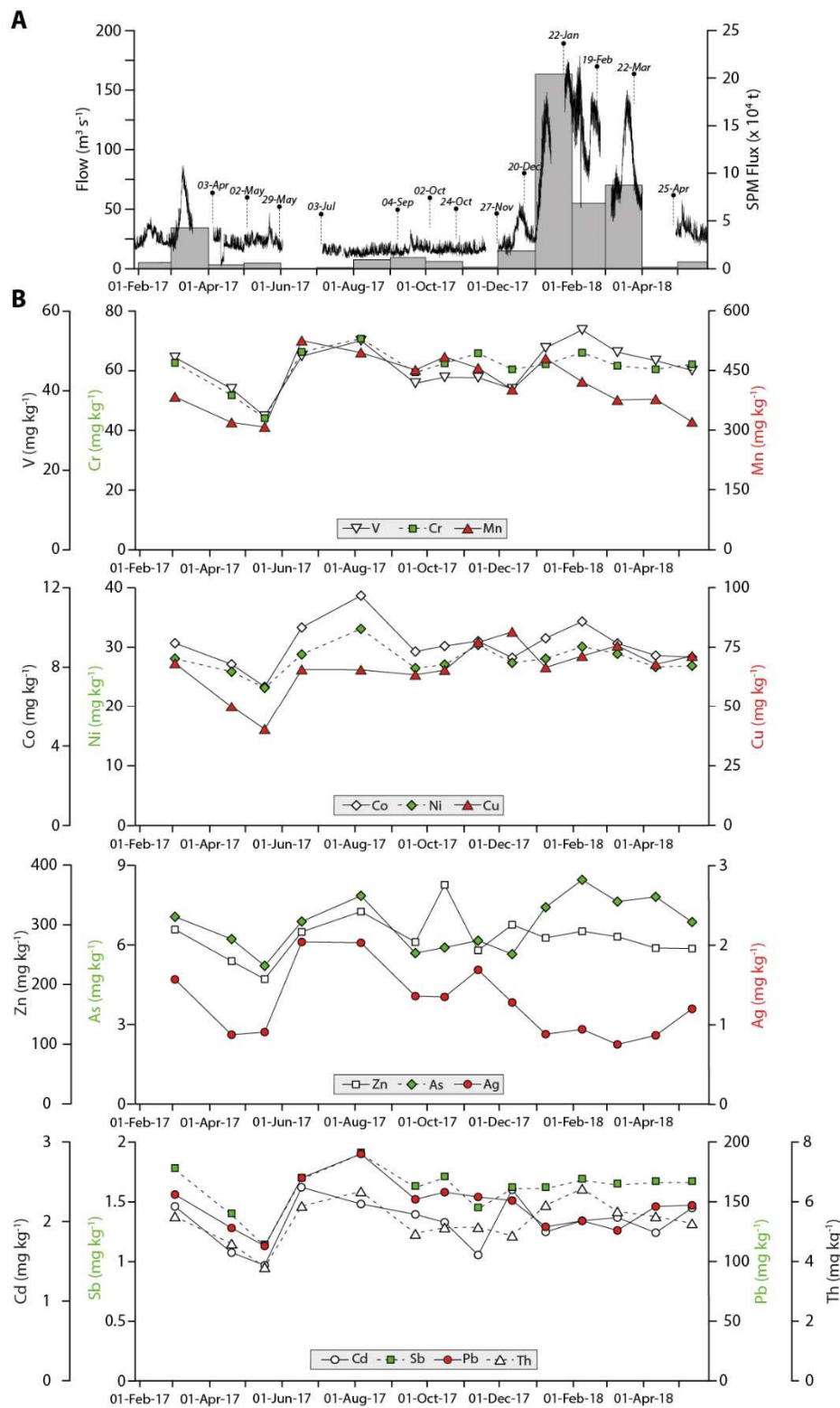


Figure 2. A. Flow ($\text{m}^3 \text{s}^{-1}$) and SPM Flux ($\times 10^4 \text{ t month}^{-1}$) at the Les Damps site; B. TMM concentrations (mg kg^{-1}) at the Les Damps site.

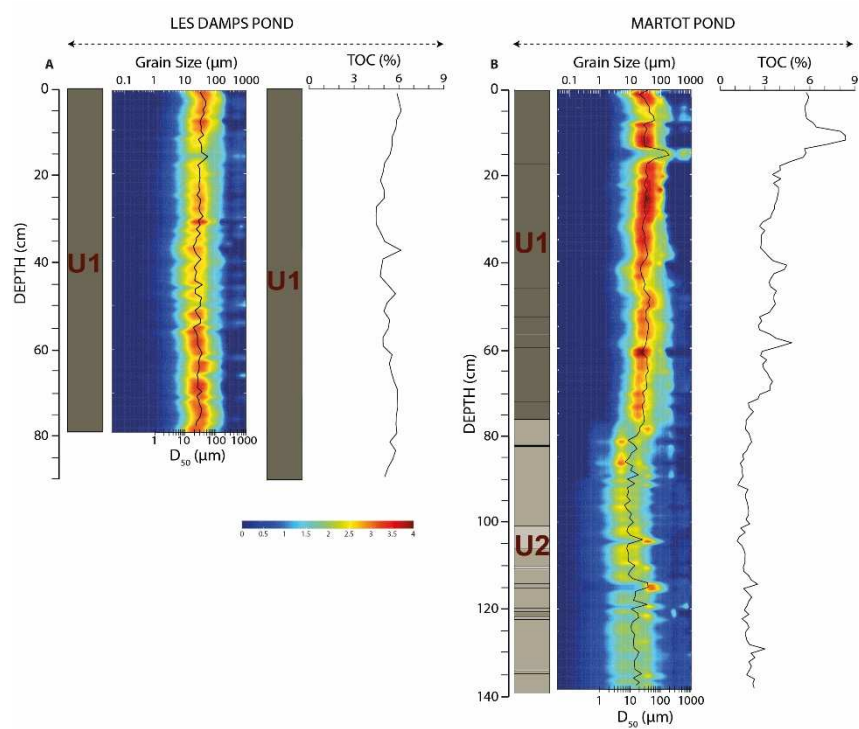


Figure 3. A. Grain size distribution, D_{50} along the DAM15-02 core and TOC along the DAM17-02 core; B. Grain size distribution, D_{50} and TOC along the MAR15-01 core.

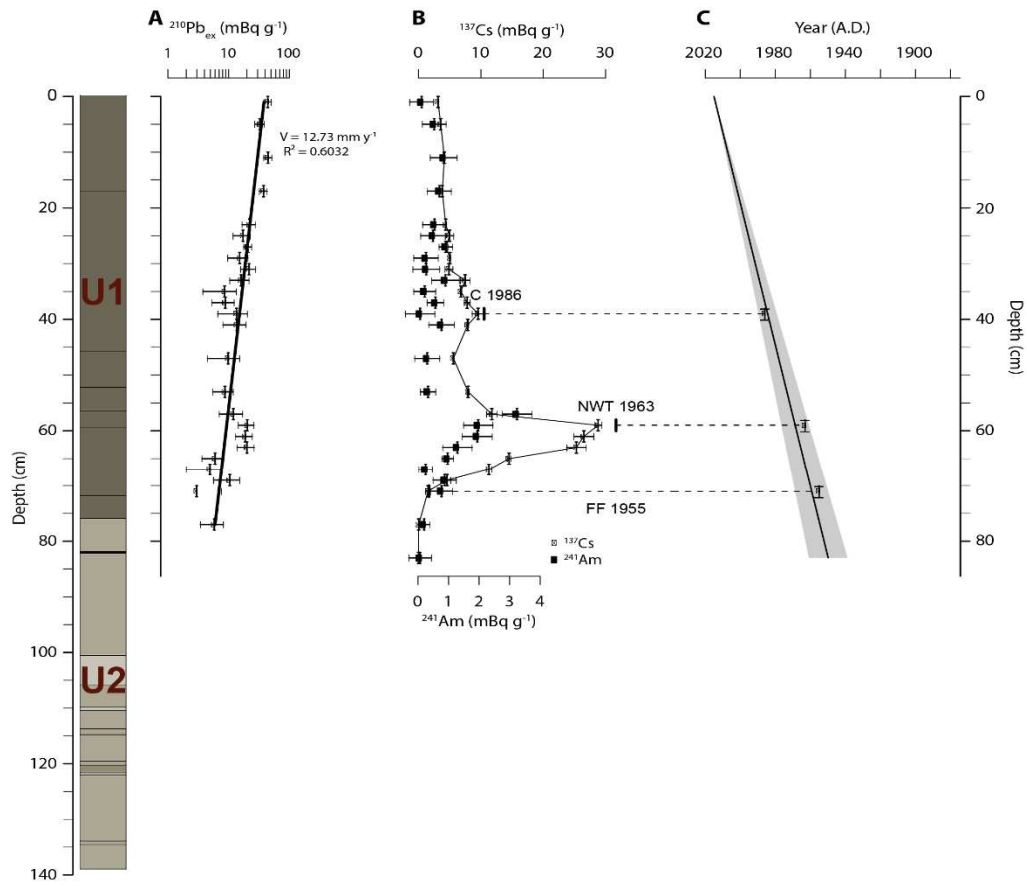


Figure 4. Age model for MAR15-01 core building with A. $^{210}\text{Pb}_{\text{ex}}$; B. ^{137}Cs and ^{241}Am (the first identification of ^{137}Cs in 1955 (FF 1955), the maximum fallout from atmospheric nuclear weapon testing in 1963 (NWT 1963) and the Chernobyl accident in 1986 (C 1986) are represented); and C. Age model.

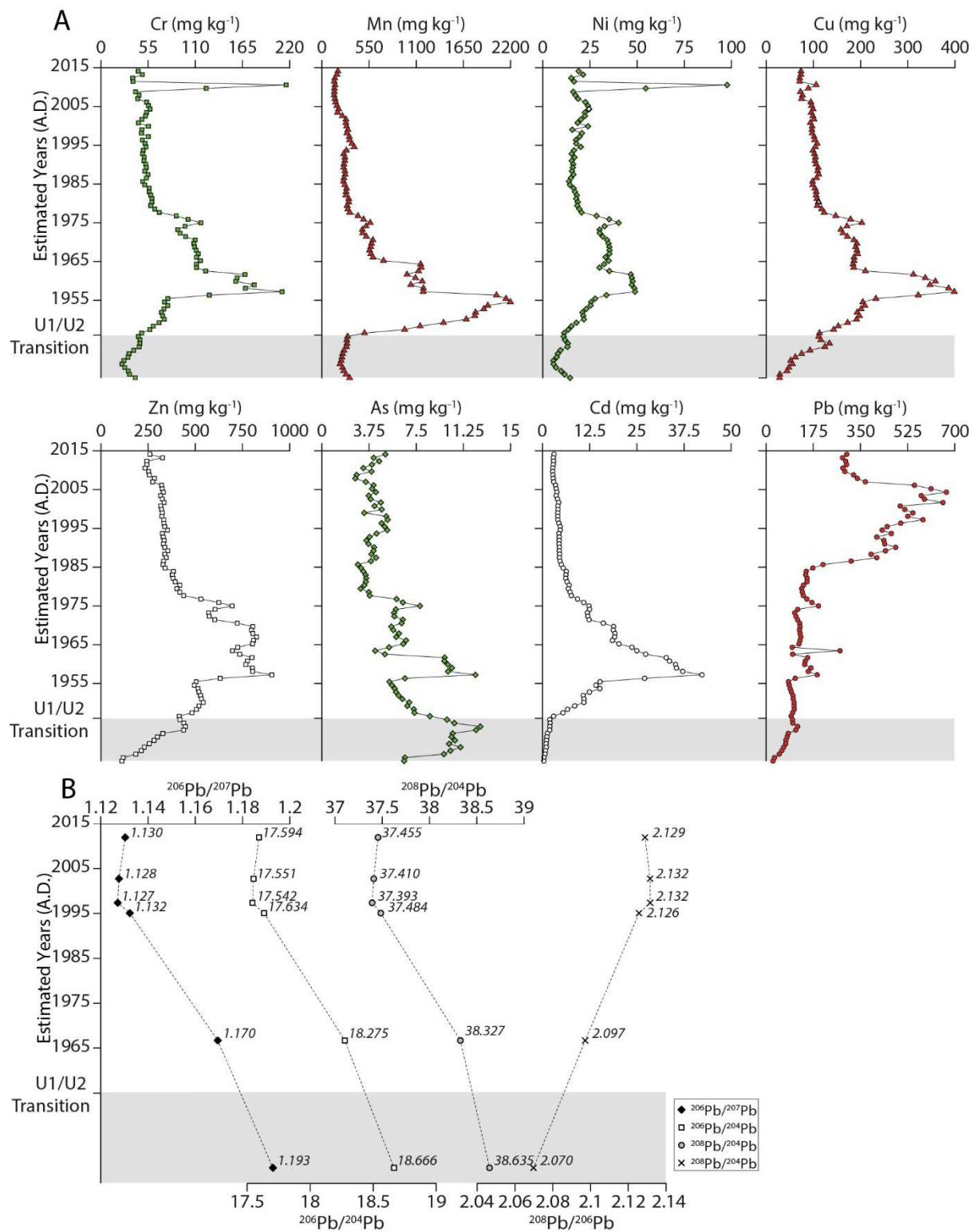


Figure 5. A. TMM concentrations along the MAR16-02 core; B. Pb isotope ratios along the MAR15-01 core (the Seine Unit U2 is represented in grey).

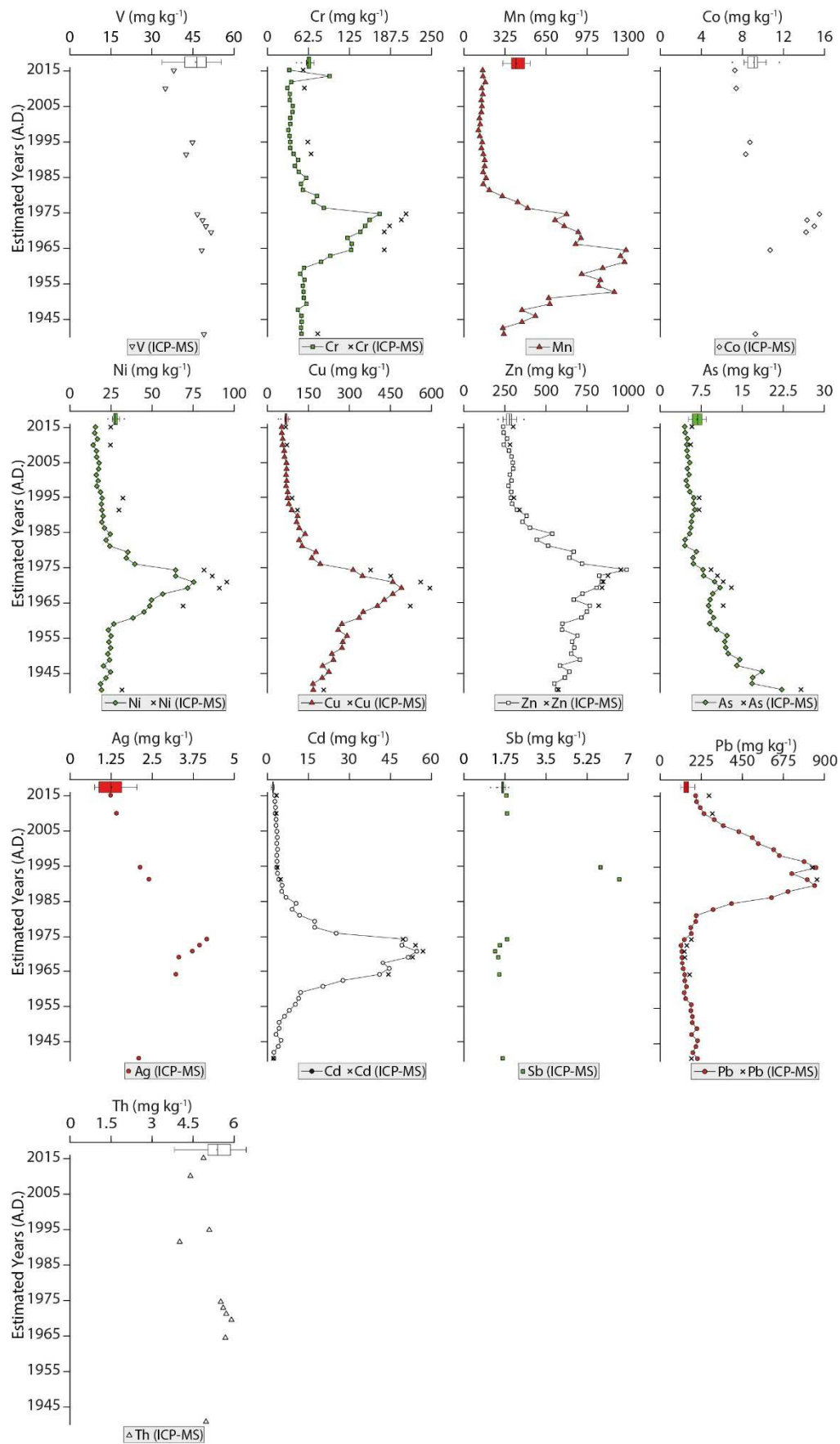


Figure 6. TMM concentrations along the DAM17-02 core. Boxplot representing TMM concentrations from SPM.

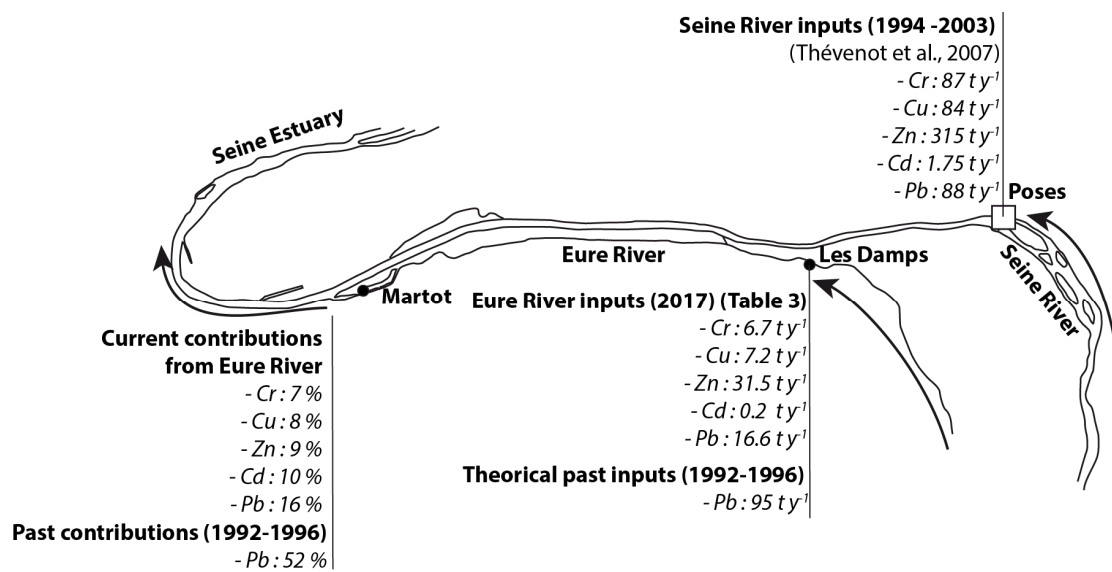


Figure 7. Eure River inputs to the Seine estuary and estimation of Eure River contributions.

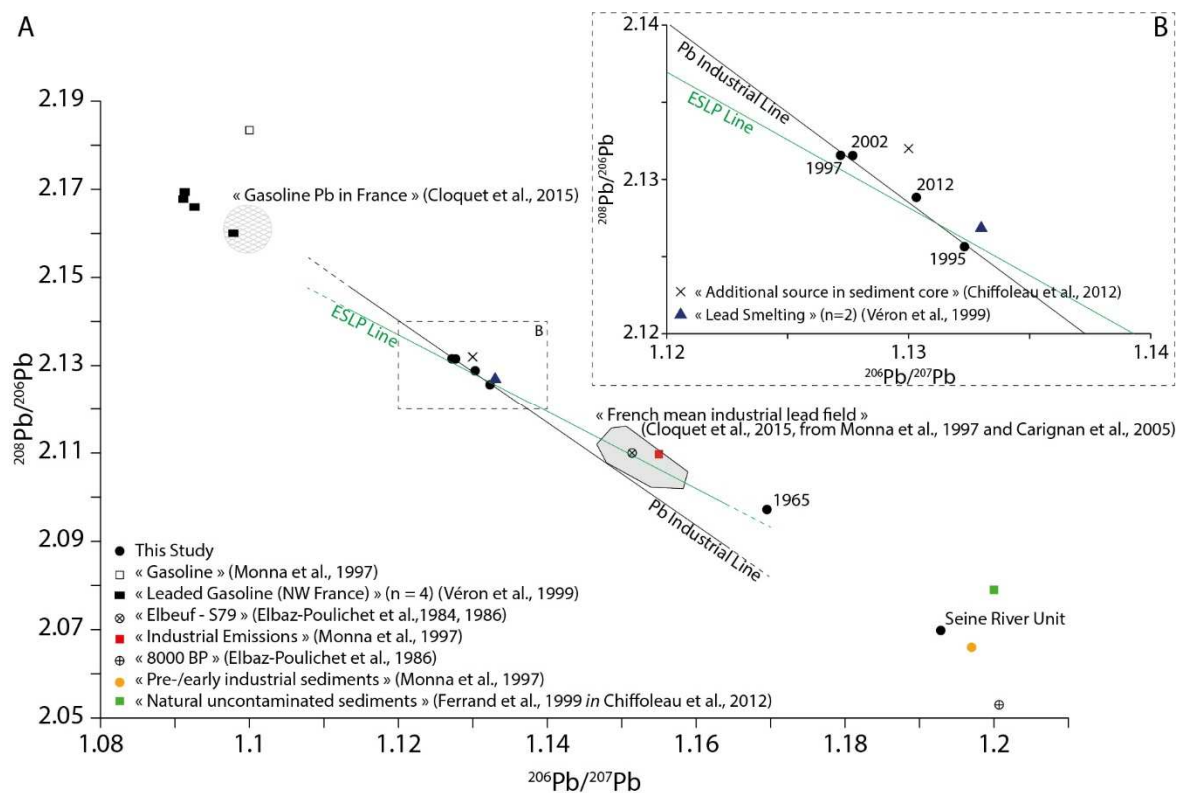


Figure 8. Three isotope diagrams $^{208}\text{Pb}/^{206}\text{Pb}$ versus $^{206}\text{Pb}/^{207}\text{Pb}$.

Table 1. Characteristics of sediment cores collected in the La Forge Pond, the Les Damps Pond and the Martot Pond (WGS 84).

Pond	Core ID	IGSN	Longitude (X)	Latitude (Y)	Core Length (cm)
LES DAMPS	DAM15-02	IEM2C0016	1°10'9.05" E	49°18'16.13" N	80
	DAM17-02	IEM2C000E	1°10'13.26" E	49°18'15.66" N	90
MARTOT	MAR15-01	IEM2C0001	1°03'1.68" E	49°17'49.68" N	138
	MAR16-02	IEM2C0008	1°03'2.60" E	49°17'49.30" N	129
LA FORGE	FOR17-02	IEM2C001D	0°37'47.89" E	48°37'51.75" N	69.5

Table 2. Age (A.D.), D₅₀ (µm), TOC (%) and TMM (mg kg⁻¹) at the bottom of the FOR17-02 core.

AGE	D ₅₀	TOC	V	Cr	Co	Ni	Cu	Zn	As	Ag	Cd	Sb	Pb	Th
1646 - 1669	20.9	2.77	43.2	32.5	5.58	9.78	5.60	32.3	6.56	0.19	0.11	0.41	10.6	3.96

Table 3. Flux of particulate TMM (kg month⁻¹) at the Les Damps site.

Sampling Interval	V	Cr	Mn	Co	Ni	Cu	Zn	As	Ag	Cd	Sb	Pb	Th
27-Jan-17 – 31-Jan-17	11.3	14.6	89.2	2.14	6.55	15.9	68.0	1.64	0.36	0.51	0.41	36.3	1.28
Feb-17	300	389	2378	57.1	175	423	1812	43.8	9.73	13.6	11.0	967	34.1
Mar-17	2065	2676	16359	393	1201	2908	12462	301	66.9	93.3	75.5	6651	235
Apr-17	166	212	1307	33.4	106	204	980	25.5	3.58	6.60	5.71	523	18.8
May-17	199	261	1830	41.3	135	240	1226	30.6	5.54	8.65	6.68	669	22.6
Jun-17	-	-	-	-	-	-	-	-	-	-	-	-	-
Jul-17	42.7	57.5	402	9.40	26.9	53.2	261	6.37	1.65	1.81	1.54	155	5.16
Aug-17	484	651	4549	106	304	602	2957	72.2	18.6	20.4	17.5	1751	58.4
Sep-17	497	704	5344	104	314	750	3214	67.5	16.2	24.8	19.2	1800	59.8
Oct-17	328	475	3634	68.8	208	504	2654	44.9	10.5	14.8	12.6	1190	39.0
Nov-17	74.5	113	782	16.2	52.3	134	450	10.6	2.87	2.85	2.52	266	8.88
Dec-17	843	1147	8165	167	519	1402	5437	120	20.7	40.6	30.1	2646	99.5
Σ_{2017}	5010	6701	44839	999	3047	7236	31521	724	157	228	183	16653	582
Jan-18	10904	13155	90856	2028	5972	14137	58065	1637	187	398	336	26908	1267
Feb-18	3757	4505	28591	698	2058	4926	19793	574	63.4	138	115	9138	436
Mar-18	4332	5390	32852	801	2511	6568	24403	669	66.6	178	144	11131	495
Apr-18	73.4	101	522	13.9	43.8	116	424	11.2	1.95	3.54	2.70	240	8.60
01-May-18 – 22-May-18	304	419	2160	57.3	181	481	1755	46.2	8.08	14.7	11.2	992	35.6

Table 4. TMM concentrations (mg kg⁻¹) in the DAM17-02 core (ICP-MS).

Sampling Depth (cm)	V	Cr	Co	Ni	Cu	Zn	As	Ag	Cd	Sb	Pb	Th
1	38.0	54.4	7.26	24.8	67.1	300	5.81	1.23	3.34	1.81	268	4.88
7	34.9	56.3	7.39	24.6	71.6	281	5.58	1.41	3.24	1.84	286	4.40
25	44.8	61.5	8.73	32.2	90.2	305	7.13	2.13	3.61	5.82	833	5.09
29	42.5	66.5	8.32	29.8	110	339	7.13	2.40	4.84	6.62	859	4.01
49	46.6	211	15.5	81.6	377	956	9.31	4.16	49.6	1.84	171	5.51
51	48.5	204	14.3	86.6	451	877	10.47	3.94	54.1	1.53	146	5.60
53	49.7	186	15.0	95.5	560	849	11.54	3.72	56.9	1.33	133	5.71
55	51.6	178	14.2	91.0	594	841	13.03	3.31	53.1	1.46	135	5.90
61	48.2	178	10.7	68.9	523	821	11.54	3.22	44.2	1.51	161	5.68
89	49.0	76.6	9.26	31.7	206	576	25.74	2.09	2.25	1.65	171	4.97

Table 5. Enrichment Factor (EF) based on the reference level from the DAM17-02 core (EF_{DAM}) and the geochemical background of the Eure River Watershed (EF_{FOR}).

Depth (cm)	Cr		Co		Ni		Cu		Zn		As		Ag		Cd		Sb		Pb	
	EF _{DAM}	EF _{FOR}	EF _{DAM}	EF _{FOR}	EF _{DAM}	EF _{FOR}	EF _{DAM}	EF _{FOR}	EF _{DAM}	EF _{FOR}	EF _{DAM}	EF _{FOR}	EF _{DAM}	EF _{FOR}	EF _{DAM}	EF _{FOR}	EF _{DAM}	EF _{FOR}	EF _{DAM}	EF _{FOR}
1	1.0	1.4	1.00	1.1	1.0	2.1	1.0	9.7	1.0	7.5	1.0	0.7	1.0	5.2	1.5	24	1.1	3.6	1.6	21
7	1.1	1.6	1.1	1.2	1.1	2.3	1.2	12	1.0	7.8	1.1	0.8	1.3	6.6	1.6	26	1.3	4.0	1.9	24
25	1.1	1.5	1.2	1.2	1.2	2.6	1.3	13	1.0	7.3	1.2	0.8	1.7	8.7	1.6	25	3.4	11	4.7	61
29	1.5	2.0	1.4	1.5	1.5	3.0	2.0	20	1.4	10	1.5	1.1	2.4	12	2.7	42	5.0	16	6.2	80
49	3.4	4.7	1.9	2.0	2.9	6.0	5.0	48	2.8	21	1.4	1.0	3.0	16	20	313	1.0	3.2	0.9	12
51	3.3	4.4	1.7	1.8	3.0	6.3	5.9	57	2.5	19	1.6	1.1	2.8	15	21	336	0.8	2.6	0.8	10
53	2.9	4.0	1.8	1.9	3.3	6.8	7.1	69	2.4	18	1.7	1.2	2.6	14	22	346	0.7	2.2	0.7	8.7
55	2.7	3.7	1.6	1.7	3.0	6.2	7.3	71	2.3	17	1.9	1.3	2.2	12	20	312	0.7	2.4	0.7	8.6
61	2.8	3.8	1.3	1.3	2.4	4.9	6.7	65	2.3	18	1.7	1.2	2.2	12	17	270	0.8	2.6	0.8	11
89	1.4	1.9	1.3	1.3	1.3	2.6	3.0	29	1.9	14	4.4	3.1	1.7	9	1.0	16	1.0	3.2	1.0	13

